# Extrafollicular responses are sufficient to drive initiation of autoimmunity and early disease hallmarks of lupus

Lasse F. Voss[1,2], Amanda J. Howarth[1], Thomas R. Wittenborn[1], Sandra Hummelgaard[1], Kristian Juul-Madsen[1], Kristian S. Kastberg[1], Mathias K. Pedersen[1], Lisbeth Jensen[1], Anastasios D. Papanastasiou[3], Thomas Vorup-Jensen[1], Kathrin Weyer[1], and Søren E. Degn[1*]

[1]Department of Biomedicine, Aarhus University, Aarhus, Denmark
[2]Department of Health Technology, Technical University of Denmark, Kongens Lyngby, Denmark
[3]Department of Biomedical Sciences, University of West Attica, Athens, Greece
[*]Corresponding author: sdegn@biomed.au.dk

Keywords: Autoimmunity, Germinal Centers, Extrafollicular Responses, B Cells, Autoantibodies, Systemic Lupus Erythematosus.

# Summary (39/40)

Affinity-matured autoantibodies generated in germinal centers are a hallmark of autoimmune diseases. Voss et al. block germinal centers in two autoimmune models, but surprisingly find that disease progresses unimpeded. They identify the extrafollicular pathway as a 'backdoor to autoimmunity'.

# Abstract (160/160)

Many autoimmune diseases are characterized by germinal center (GC) derived affinity-matured, class-switched autoantibodies. Strategies to block GC formation and progression are currently being explored clinically, however, extrafollicular responses may also contribute to early events in autoimmunity. To investigate the relative contribution of these two pathways in autoimmune disease development, we leveraged a transgenic strategy to genetically block the GC pathway. Surprisingly, this accelerated extrafollicular responses and failed to curb autoimmune progression in two lupus models. *In vitro*, loss of the GC transcription factor Bcl-6 prevented cellular expansion and accelerated plasma cell differentiation, suggesting the *in vivo* phenotype was caused by rewiring of B cell intrinsic transcriptional programming. In a competitive scenario *in vivo*, B cells harboring the genetic GC block contributed disproportionately to the plasma cell output. Taken together, this emphasizes the extrafollicular pathway as a key contributor to autoimmune progression, and suggests that strategies aimed at blocking GCs should simultaneously target this pathway to avoid rerouting the pathogenic response.


**Highlights:**

-A genetic GC block fails to prevent autoimmune progression in two lupus models
-An intrinsic GC block drives B cell differentiation into terminally differentiated plasma cells *in vitro*
-B cells harboring a GC block competitively contribute to the plasma cell compartment in an autoreactive setting *in vivo*
-Lupus mice with a GC block display immune complex deposition in kidney glomeruli that is indistinguishable from their wild-type counterparts

# Introduction

Many autoimmune diseases, such as systemic lupus erythematosus (SLE) and Sjögren's syndrome, are characterized by the development of autoantibodies targeting nuclear antigens (Psianou et al., 2018; Rahman and Isenberg, 2008). Such antibodies can be produced by B cells via two routes, the extrafollicular pathway and the germinal center (GC) pathway (Elsner and Shlomchik, 2020). The extrafollicular pathway leads to the rapid expansion and differentiation of B cells to plasmablasts (PBs) and short-lived plasma cells (PCs), which in a natural infection setting provides rapid initial protection against pathogens. The GC pathway is slower, but enables a higher-quality response characterized by extensive somatic hypermutation and affinity maturation, robust memory cell generation, and production of long-lived PCs (Victora and Nussenzweig, 2022). At an individual B cell level, the decision between extrafollicular and GC pathway differentiation appears to rest on the initial affinity for antigen (Paus et al., 2006). While both pathways can support class-switch recombination and affinity maturation, the antibody class diversity and extent of somatic hypermutation is much greater through the GC pathway (Sweet et al., 2010; William et al., 2002).

Upon initial activation of B cells by their cognate antigen, they can either T-independently or T-dependently form an extrafollicular focus. Here they proliferate, as well as potentially class-switch, and may additionally undergo a low degree of somatic hypermutation, before they differentiate into PCs. In the context of autoimmune diseases, it has been noted that initial B cell reactivities often target autoantigenic components that carry endogenous TLR ligands capable of stimulating them independently of T cells (Lau et al., 2005; Leadbetter et al., 2002; Sweet et al., 2011). Of note, these seem strictly limited to components topologically linked to the B cell receptor (Green et al., 2021). Interestingly, signals that drive initial B cell activation also seem to limit the extent of affinity maturation (Akkaya et al., 2018). However, as autoimmune disease progresses, the breadth of the autoantigenic response often broadens, leading to inclusion of T-dependent reactivities (Cornaby et al., 2015). In both humans and mice, this broadening of the response, termed epitope spreading, has been observed even before the onset of clinical symptoms (Arbuckle et al., 2003; Degn et al., 2017b).

Epitope spreading is thought to occur through the GC pathway. In this alternate outcome of initial B cell activation, the B cells may form a primary focus in the interfollicular region, where they undergo limited proliferation and may class-switch (Roco et al., 2019; Toellner et al., 1996). They then subsequently co-migrate with cognate T cells into the follicle, where they can form a GC. In the GC, the B cells proliferate rapidly and form a 'dark zone', and are now termed centroblasts (Victora and Nussenzweig, 2022). The centroblasts undergo somatic hypermutation to diversify their B cell receptors. They subsequently migrate to the 'light zone', where they scan follicular dendritic cells for antigen. The B cells that display the highest affinity for antigen can competitively acquire antigen and present derived peptides to T follicular helper ($T_{FH}$) cells. B cells that receive cognate T cell help may return to the dark zone for another round of division and hypermutation. B cells that do not receive help perish through programmed cell death and are engulfed by tingible body macrophages (Victora and Nussenzweig, 2022). Due to the power of the GC pathway, and the risk for inadvertent emergence of novel (auto)reactivities that are distinct from the original antigenic target, it is subject to stringent control. The requirement for T cell selection subsequent to every successive round of hypermutation, a phenomenon termed linked recognition, restricts inadvertent broadening of the response. An additional layer of control appears to be exerted

by a specialized subset of T regulatory cells, termed T follicular regulatory ($T_{FR}$) cells (Fahlquist Hagert and Degn, 2020). Nonetheless, these mechanisms appear to fail in autoimmune disease, which frequently display rampant GC activity (Domeier et al., 2017; Luzina et al., 2001).

Hence, we hypothesized that the GC pathway is critical to the autoimmune process, and that a genetic block of the GC pathway *in vivo* would prevent autoimmune development. To our surprise, a global block in the GC pathway *in vivo* in two independent models did not ameliorate autoimmune disease, but if anything exacerbated it. In an *in vitro* GC B cell culture system, GC blocked B cells expanded to a lesser extent, but were found to more rapidly develop into PBs and PCs. In a competitive scenario *in vivo*, GC blocked B cells competed efficiently with their wild-type counterparts, disproportionate to their inability to participate in GCs. Our determination of the relative contributions of the extrafollicular and GC pathways to autoimmune progression highlight a critical role of extrafollicular responses in driving autoimmune development.

# Materials and methods

**Mice**

The Bcl-6$^{flx/flx}$ strain (Hollister et al., 2013) and congenic B6.CD45.1 (B6.SJL-Ptprc$^{a}$ Pepc$^{b}$/BoyJ) were purchased from Jackson Laboratories (stock no. 023737 and 002014, respectively). Aicda-Cre transgenic mice (Kwon et al., 2008) were kindly provided by Meinrad Busslinger, The Research Institute of Molecular Pathology (IMP), Vienna. Aicda-Cre and Bcl-6$^{flx/flx}$ strains were intercrossed to generate Aicda-Cre+ and Aicda-Cre- Bcl-6$^{flx/flx}$ littermates. 564Igi mice (Berland et al., 2006) (B6.Cg-Igh$^{tm1(Igh564)Tik}$Igk$^{tm1(Igk564)Tik}$/J) were kindly made available by Theresa Imanishi-Kari, Tufts University, and provided by Michael C. Carroll, Boston Children's Hospital. The 564Igi line was crossed to Aicda-Cre Bcl6$^{flx/flx}$ to generate 564Igi H$^{+/+}$ K$^{+/+}$ Aicda-Cre+/- Bcl6$^{flx/flx}$ littermates. Mice were housed in the Animal Facility at the Department of Biomedicine, Aarhus University, Denmark, under specific pathogen-free (SPF) conditions, on a 12-hour light/dark cycle with standard chow and water *ad libitum*. Both male and female mice were used in experiments. Mice were between 8 and 14 weeks old upon initiation of experiments.

**Ethics Statement**

All animal experiments were conducted in accordance with the guidelines of the European Community and were approved by the Danish Animal Experiments Inspectorate (protocol numbers 2017-15-0201-01348 and 2017-15-0201-01319).

**R848 treatment protocol**

Mice were treated topically on the right ear 3 times per week for 4 weeks with 1 mg R848/mL acetone using a cotton applicator or did not receive any treatment (Untreated/Unt).

**Mixed bone marrow chimeras**

Recipient mice were irradiated with 9 Gy in a MultiRad 350 (Faxitron), with 350 kV, 11.4 mA, a Thoraeus filter [0.75 mm Tin (Sn), 0.25 mm Copper (Cu), and 1.5 mm Aluminium (Al)], and with a beam-distance of 37 cm. Irradiated recipients were kept on antibiotic water (either 1 mg sulfadiazine together with 0.2 mg trimethoprim per mL drinking water, or 0.25 mg amoxicillin per mL drinking water) to avoid any opportunistic infections. On the following day, donor mice were anesthetized with 4% isoflurane and euthanized. Femora, fibulae/tibiae, ossa coxae and humeri were harvested, mechanically cleaned and rinsed in FACS buffer. The Bone marrow (BM) cells were released from the harvested bones by crushing and the cell extract was then passed through a 70 µm cell strainer. The donor BM cells were then counted in a Cellometer K2 cell counter (Nexcelom). Cells were pelleted by centrifugation (200 *g*, 10 min, 4°C) and resuspended to $1*10^{8}$ cells/mL. Donor cells from three different mice were then mixed according to the proportions mentioned in the figure legend. The donor cell mixtures were used to reconstitute the recipient mice by retroorbital injection of 200 µL (containing a total of $20*10^{6}$ cells) into each recipient mouse. The reconstituted recipient mice were placed on antibiotic water the following 14 days.

**Tissue preparation**

Mice were anesthetized with isoflurane (055226, ScanVet), blood samples from the retroorbital plexus were collected, and mice were euthanized using 100-150 mg/kg sodium pentobarbital (450009, Dechra Veterinary Products). Mesenteric lymph nodes (MesLN) and

inguinal lymph nodes (IngLN) were removed, the splenic artery was clamped with a hemostat, and the spleen was removed. The mice were perfused intracardially with PBS (BE17-515Q, Lonza) to remove the blood, and subsequently perfused with 4% w/v paraformaldehyde (PFA) (1.04005.100, Merck) in PBS to fix the tissues. Finally, kidneys and auricular lymph nodes (AurLNs) were removed.

Collected blood samples were centrifuged at 3,000 *g* for 10 minutes, the supernatant was collected, and centrifuged again at 20,000 *g* for 3 minutes. Serum samples were stored at -20°C. The spleen and AurLNs was directly embedded in Tissue-Tek O.C.T. media (4583, Sakura Finetek) and frozen at -20°C for histology. The kidneys were kept in 4% w/v PFA for 24 hours, and then changed to 30% w/v sucrose in PBS. A small part of the spleen as well as IngLN and MesLN were stored in fluorescence-associated cell sorting (FACS) buffer (PBS, 2% heat-inactivated fetal calf serum (FCS), 1 mM ethylenediaminetetraacetic acid (EDTA)) for FACS typing.

**Flow cytometry**

Spleen, IngLN and MesLN were harvested, stored into ice-cold FACS buffer, and mechanically dissociated using pestles. Spleen and LNs were filtered through 70 $\mu$m cell strainers. Spleen samples were centrifuged at 200 *g* for 5 minutes at 4°C, lysed in RBC lysis buffer (155 mM $NH_4Cl$, 12 mM $NaHCO_3$, 0.1 mM EDTA), incubated at RT for 3 minutes, centrifuged, and finally resuspended in FACS buffer or calcium-containing buffer (PBS, 20 mM HEPES, 145 mM NaCl, 5 mM $CaCl_2$, 2% FBS) when Annexin-V was included in the panels. Samples were filtered through 70 $\mu$m cell strainers. Twenty $\mu$L Fc-block (553142, BD) diluted 1:50 in PBS and 100 $\mu$L of each sample was added onto a 96-well plate and incubated for 5-10 minutes. Antibodies and fixable viability dye (65-0865-14, ThermoFisher Scientific) were diluted in FACS buffer or calcium-containing buffer as indicated below. One hundred $\mu$L antibody mix was added to each sample well and incubated for 30 minutes on ice. The plate was centrifuged at 200 *g* for 5 minutes, supernatant was removed, and cells were fixed for 30 minutes in PBS, 0.9% formaldehyde (F1635, Sigma- Aldrich) at RT. Later, the plates were centrifuged at 200 *g* for 5 minutes, the supernatant discarded, and the samples resuspended in FACS buffer or calcium-containing buffer. Flow cytometry evaluation was performed the following day using a 4-laser (405 nm, 488 nm, 561 nm, 640 nm) LSRFortessa analyzer (BD instruments). The following antibodies and reagents were used for flow cytometry experiments: Annexin-V-AF488 (A13201, ThermoFisher Scientific, 1:500), B220-PB clone RA3-6B2 (558108, BD, 1:500), B220-PerCP-Cy5.5 clone RA3-6B2 (561101, BD Biosciences, 1:500), CD4-PerCP clone RM4-5 (100538, BioLegend, 1:500), CD8-PerCP-Cy5.5 clone SK1 (565310, BD, 1:500), CD38-PE-Cy7 clone 90 (102718, BioLegend, 1:500), CD45.1-FITC clone A20 (110706, BioLegend, 1:500), CD45.2-APC clone 104 (109814, BioLegend, 1:500), CD95-PE clone Jo2 (554258, BD, 1:500), CD138-BV650 clone 281-2 (564068, BD, 1:500), 9D11-biotin (hybridoma kindly provided by Elisabeth Alicot, Boston Children's Hospital, produced, purified and biotinylated in-house, 1:300), Ly6G/C-APC-R700 clone RB6-8C5 (565510, BD, 1:500), Viability Dye eFlour 780 (65-0865-14, Thermo Fisher Scientific, 1:2000), Streptavidin-BV786 (563858, BD Biosciences, 1:500), hCD2-PB clone RPA-2.10 (300236, BioLegend, 1:200), IgD-AF488 clone 11-26c.2a (405718, BioLegend, 1:500), IgMb-BV510 clone AF6-78 (742344, BD OptiBuild, 1:500), TACI-AF647 clone 8F10 (558453, BD Biosciences, 1:500), CD45.2-BV786 clone 104 (563686, BD Horizon, 1:500), CD19-AF700 clone 1D3 (557958, BD Pharmingen, 1:500).

**Quantum Dot coupling of antibody**

Quantum Dot (QD) antibody coupling was done using SiteClick Qdot 655 Antibody Labeling Kit (Molecular Probes, S10453) according to manufactures instructions. In brief, antibody (either "14D12" rat IgG2a to mouse MBL-C (Hycult Biotech), or "RTK2758" rat IgG2a isotype control (Abcam)) was concentrated in antibody preparation buffer to a concentration of 2 mg/mL or above. Next, carbohydrates on the antibody were modified by the incubation with β-galactosidase for 4 h at 37°C. Azide modification was achieved through incubation with uridine diphosphate glucose-GalT enzyme overnight at 30°C. Antibody with modified carbohydrates was purified and concentrated through a series of centrifugation steps using a molecular-weight cutoff membrane concentrator, and the buffer was simultaneously changed to 20 mM Tris, pH 7.0. Finally, 5′-dibenzocyclooctyne-modified QD nanocrystals were coupled overnight at 25°C and stored at 4°C until further use.

**Nanoparticle Tracking Analysis**

Samples for Nanoparticle Tracking Analysis (NTA) were analyzed using a NanoSight NS300 system (Malvern Panalytical) as previously described (Juul-Madsen et al., 2021). The system was configured with a 405 nm laser, a high-sensitivity scientific complementary metal–oxide–semiconductor Orca Flash 2.8/Hamamatsu C11440 camera (Malvern Panalytical), a syringe pump, and for fluorescence measurements, a 650 nm long-pass filter was used. The sample chamber was washed twice with 1 mL PBS with 1 mM EDTA (PBS/EDTA) before each measurement. All samples were thoroughly mixed before measurement and were injected into the sample chamber using 1-mL syringes. The measurement script comprised temperature control at 23°C, followed by a 20 s flush at a flowrate mark 1000. Next, sample advancement was stabilized by a 120 s advancement at flowrate mark 10. Recordings were captured continuously during a steady flow at flowrate mark 10 with five 60-s recordings separated by 5-s lag time between each sample. The videos were collected and analyzed using NanoSight software (version 3.4 with a concentration upgrade; Malvern). Automatic settings were used for the minimal expected particle size, minimum track length, and blur setting. Camera sensitivity and detection threshold were adjusted according to sample composition and kept constant for all samples to be directly compared. For fluorescence mode, the camera level was set to maximum (mark 16), and the detection threshold was set to minimum (mark 2). Serum samples from mice were analyzed in a 1:20 dilution in PBS/EDTA with a 1:20,000 dilution of MBL-C–specific (14D12) or isotype Antibody-QD reporters. A 50 nm cutoff was established for all samples to exclude unbound QD conjugates as well as QD conjugates bound to smaller forms of MBL-C.

**Immunohistochemical labelling of kidney tissue**

After perfusion fixation, kidneys were stored in PBS with 30% sucrose and 0.1% sodium azide. For paraffin-embedding, the kidneys were washed in 10 mM PBS several times, dehydrated in 70%, 96%, and 99% ethanol for 2 hours, respectively, before they were transferred to xylene overnight. The day after, kidneys were embedded in paraffin. Paraffin embedded kidney sections (2 µm) were cut on a Leica RM 2165 microtome (Leica, Wetzlar, Germany) and dried at 60°C for 1 h. For immunofluorescent (IF) labelling, sections were placed in xylene overnight, rehydrated in graded alcohols, and heated in TEG buffer (10 mM Tris, 0.5 mM EGTA buffer, pH 9) at ~100°C for 10 min to induce epitope retrieval. Sections were subsequently cooled for 30 min, incubated in 50 mM $NH_4Cl$ in 0.01 mM PBS for 30 min, and incubated at 4°C with primary antibody overnight. The following day, sections were washed, incubated with secondary antibody for 1 h, and coverslips were mounted using mounting medium (Dako

255 fluorescence Mounting medium, #S3023). Immunofluorescent images were acquired by a
256 confocal laser-scanning microscope (LSM 800 with Airyscan, Carl Zeiss Gmbh, Jena, Germany)
257 and processed using ZEN lite 3.4 (Blue edition). For immunoperoxidase (IP) labelling, sections
258 were prepared as stated above. In addition, endogenous peroxidase was blocked by placing
259 sections in 30% $H_2O_2$ in methanol for 30 min and peroxidase-conjugated secondary antibodies
260 were used. Furthermore, the sections were incubated with DAB, counterstained with Mayer's
261 haematoxylin (Sigma-Aldrich), dehydrated in graded alcohols, cleared in xylene and mounted
262 with coverslips using Eukitt (Sigma-Aldrich). For periodic acid-Schiff (PAS) stainings, sections
263 were incubated in 1% periodic acid for 10 min and treated with Schiff's reagent for 20 min.
264 Subsequently, all sections were counterstained with Mayer's hematoxylin for 5 min and
265 mounted with coverslips using Eukitt. Peroxidase-labelled and PAS-stained images were
266 collected by a Leica DFC320 camera (Leica, Wetzlar, Germany). H&E and PAS stained kidney
267 sections were scored by a histopathologist, blinded to the identity of the samples. High-
268 resolution images of kidney and spleen sections were obtained using a Zeiss LSM 800 Airyscan
269 confocal microscope with 4 lasers (405 nm, 488 nm, 561 nm, 640 nm). ZEN software was used
270 for quantification of immunofluorescence kidney stainings. The following primary antibodies
271 were used: anti-C3 (ab11887, Abcam, 1:25 (IP), 1:50 (IF)), anti-IgG2c (1079-08,
272 SouthernBiotech, 1:25 (IF), 1:50 (IP)), anti-Nephrin (GP-N2, Progen, 1:100), anti-Ig (1010-08,
273 SouthernBiotech, 1:100 (IF), 1:200 (IP)). The following secondary antibodies were used:
274 Donkey-a-rabbit AF488 (A21206, ThermoFisher, 1:300), Streptavidin AF647 (405237,
275 BioLegend, 1:500), Goat-a-Guinea Pig AF488 (A11073, ThermoFisher, 1:300), Goat-a-rabbit
276 HRP (P0448, Dako, 1:200), Streptavidin HRP (P0397, Dako, 1:200)
277
278 **Time-resolved immunofluorometric analysis (TRIFMA) anti-dsDNA measurements**
279 A FluoroNunc Maxisorp 96-well plate was coated with 100 µg/mL salmon sperm dsDNA
280 (AM9680, Invitrogen) in PBS and incubated overnight at 4°C. Wells were blocked with 200 µL
281 TBS containing 1% bovine serum albumin (BSA) (A4503, Sigma-Aldrich) for 1 hour at RT and
282 washed 3 times with TBS/Tw (TBS containing 0.05% v/v Tween-20 (8.17072.1000, Merck)).
283 Samples, standards and quality controls were diluted in TBS/Tw containing 5 mM EDTA and
284 0.1% w/v BSA, and were subsequently loaded onto the plate in duplicates. The plate
285 incubated at 37°C for 1 hour. Then, wells were washed 3 times in TBS/Tw and incubated with
286 biotinylated antibody (Table 2.5) at 37°C for 1 hour. Wells were washed 3 times in TBS/Tw,
287 and $Eu^{3+}$-tagged streptavidin (1244-360, PerkinElmer) diluted 1:1,000 in TBS/Tw containing
288 25 µM EDTA were subsequently added to the wells and incubated at RT for 1 hour. Finally,
289 the wells were washed 3 times in TBS/Tw, 200 µL enhancement buffer (AMPQ99800,
290 Amplicon) was added. The plate was shaken for 5 minutes and counts were read by a time-
291 resolved fluorometry plate reader Victor X5 (Perkin Elmer).
292
293 **TRIMA Ig measurements**
294 A FluoroNunc Maxisorp 96-well plate was coated with 1 µg/mL goat anti-mouse Ig in PBS and
295 incubated overnight at 4°C. Wells were blocked in 1 mg HSA/mL TBS for 1 hour at RT and
296 washed 3 times with TBS/Tw. Samples, standards and quality controls, diluted in TBS/Tw
297 containing 100 µg/mL heat-aggregated human Ig, were subsequently loaded onto the plate
298 in duplicates, and incubated overnight at 4°C. The wells were washed 3 times with TBS/Tw,
299 and 1 µg/mL biotinylated goat anti-mouse Ig was added to the wells and incubated for 2 hours
300 at RT. Wells were washed 3 times in TBS/Tw, and $Eu^{3+}$-tagged streptavidin (1244-360,
301 PerkinElmer) diluted 1:1,000 in TBS/Tw containing 25 µM EDTA were subsequently added to

302 the wells and incubated at RT for 1 hour. Finally, the wells were washed 3 times in TBS/Tw,
303 200 µL enhancementbuffer (AMPQ99800, Amplicon) was added. The plate was shaken for 5
304 minutes and counts were read by a Victor X5 time-resolved fluorometry plate reader (Perkin
305 Elmer).
306
307 **Immunofluorescence staining of spleens and auricular lymph nodes**
308 A Cryostar NX70 Cryostat (ThermoFisher) was used to cut 16 µm thick spleen sections or 20
309 µm thick auricular lymph node sections which were mounted on SuperFrost+ glass slides
310 (Fisher Scientific). Spleen sections were either acetone or PFA fixed, auricular lymph nodes
311 were PFA fixed. For acetone fixation, the spleen samples were rinsed in PBS and fixed in
312 acetone for 10 minutes at room temperature (RT), whereafter the slides were rehydrated in
313 PBS for 3 minutes. For PFA fixation protocols, the slides were washed in PBS, fixed with 4%
314 w/v PFA for 30 min at RT, incubated in TBS (10 mM Tris, 140 mM NaCl, pH 7.4) for 30 min at
315 RT, rinsed briefly with PBS, and incubated with permeabilization buffer (PBS, containing 2%
316 v/v FBS, 0.1% w/v sodium azide, 0.1% v/v Triton-X100) for 45 minutes at RT. Antibodies were
317 diluted in staining buffer (PBS, 2% v/v FBS, 0.1% w/v sodium azide). The antibody mix was
318 centrifuged at 10,000 *g* for 5 minutes and added onto the spleen samples, where it incubated
319 overnight at 4°C. The slides were washed once with staining buffer for 5 minutes and washed
320 3 times in PBS with 0.01% v/v Tween-20 for 5 minutes. Slides were spot-dried and mounted
321 using Fluorescence Mounting Medium (S3023, Dako). Imaging for quantification of GC
322 formation was performed using an Olympus VS120 Upright Widefield fluorescence slide
323 scanner equipped with a digital monochrome camera (Hamatsu ORCA Flash4.0V2) and a 2/3"
324 CCD camera, as well as single-band exciters and a filter wheel with single-band emitters
325 (Hoechst, FITC, Cy3, Cy5, and Cy7). Fiji v. 2.1.0/1.53c was used for image processing. The
326 following antibodies were used: CD45.1-FITC clone A20 (110706, BioLegend, 1:300), CD45.2-
327 APC clone 104 (109814, BioLegend, 1:300), CD138-PE clone 281-2 (142504, BioLegend, 1:500),
328 CD169-PE clone 3D6.112 (142404, BioLegend, 1:500), IgD-AF488 clone 11-26c.2a (405718,
329 BioLegend, 1:500), Ki67-eflour660 clone SolA15 (50-5698-82, Thermo Fisher Scientific, 1:500),
330 CD21/35-PB clone 7E9 (123414, BioLegend, 1:500). Channel intensities were adjusted for
331 visual clarity in represented micrographs, but quantification was performed on raw images
332 throughout.
333
334 **Purification of B cells**
335 The spleen was harvested, stored in MACS buffer (PBS, 2% FBS, 2 mM EDTA), the cells were
336 mechanically dissociated and filtered through 70 µm cell strainers, whereafter the cell
337 suspension was topped up with MACS buffer until 25 mL and filtered through 70 µm cell
338 strainers again. The cell suspension was centrifuged at 200 *g* for 10 minutes at 4°C,
339 resuspended in 5 mL RBC lysis buffer (155 mM $NH_4Cl$, 12 mM $NaHCO_3$, 0.1 mM EDTA), and
340 incubated for 3 minutes at RT. The reaction was stopped by adding 47 mL MACS buffer, and
341 centrifuged at 200 *g* for 5 minutes at 4°C. The supernatant was discarded and resuspended in
342 3 mL MACS buffer. B cell kit (Miltenyi Biotec, 130-090-862) was followed according to the
343 manufacturer's protocol.
344
345 **iGB cultures**
346 NB21 feeder cells, kindly provided by Garnett Kelsoe, Duke University (Kuraoka et al., 2016),
347 were seeded into 6-well plates at a density of 520 cells/cm$^2$ for IL-4 stimulated wells and 5200
348 cells/cm$^2$ for the four other conditions. The following day (day 0), B cells were purified

349 according to the described protocol, and resuspended in B cell medium (BCM) (RPMI-1640
350 supplemented with 10% FCS, 55 µM 2-ME, 1% Pen/Strep, 1% MEM NEAA, 10 mM HEPES, 1
351 mM Sodium Pyruvate). B cells were pre-diluted in BCM with the given cytokine cocktail as
352 indicated in figure legends. From day 2-8, 2/3 of the total volume of BCM was collected and
353 fresh BCM was added to reach the same final volume. One mL of medium from each well of
354 the 6 well plates was collected on the final day (day 10) for TRIFMA analyses. Cells were
355 analyzed using flow cytometry, as described above. IL-4 (214-14, PeproTech) were used for
356 stimulation
357
358 **Statistical analyses**
359 GraphPad Prism v. 8.4.3 was used for statistical analyses. For each dataset, both tests for
360 normality (such as Shapiro Wilk's test) and Q-Q plots were used to determine whether the
361 data were normally distributed. Data that were not normally distributed were log-
362 transformed and re-tested for normality. The following data sets were log-normally
363 distributed: Fig 1B, 1D, 1E, 1N, 1P, 3F, 5C, 5F, 5G, 5H, 6H, 6L-O, S6L-O. For Fig 6B, 6G, S6D-S6E,
364 and S6H, Mann-Whitney test was used to analyze the data that were not normally distributed.
365 All other datasets were normally distributed, except for the data in Figure 1L, 5F, and S6K
366 which were neither normally, nor log-normally distributed. However, a non-parametric t-test
367 for the isolated data between each group in panel 1L, 5F and S6K showed similar results (for
368 Fig 1L: a significant increase in GC formation in Cre- between Unt and R848. For Fig 5F: a
369 significant increase in CD8 frequencies in the IngLNs but not in other tissues. For S6K: slight,
370 but significant increases across spleen, IngLN and blood, with a trend towards an increase in
371 MesLN when tissues are analyzed individually), indicating that the observed differences,
372 beyond being biologically robust and in agreement with the flow data, were also statistically
373 robust. Parametric tests were used in all analyses, with specific tests indicated in the figure
374 legends. All data is presented as bar graphs with mean ± SD. A p-value $<0.05$ was considered
375 to be statistically significant. ns = $p \geq 0.05$, * = $p<0.05$, **= $p<0.01$, *** = $p<0.001$.

# Results

**Genetic GC block exacerbates autoimmune progression in a lupus model**

Chronic epicutaneous application of the synthetic, small-molecule TLR7 agonist, R848 (Resiquimod), has previously been demonstrated to induce a robust lupus-like autoimmune phenotype in multiple genetic background strains of *Mus musculus* (Yokogawa et al., 2014). Leveraging this model, we set out to investigate the relative importance of the extrafollicular and GC pathways in the autoimmune response. To this end, we employed a transgenic Cre driver line displaying expression of Cre under the Aicda promotor (Kwon et al., 2008). We combined this with a conditional Bcl-6 knock-out line (Hollister et al., 2013), to achieve deletion of Bcl-6 specifically in GC B cells. As Bcl-6 is a master transcriptional regulator of the GC fates across GC B cells, $T_{FH}$ cells and $T_{FR}$ cells, this approach specifically prevents GC B cell differentiation, without affecting Bcl-6 dependent T cell subsets essential to support both GC and extrafollicular responses (Lee et al., 2011). As controls, we employed Cre negative Bcl-$6^{flx/flx}$ littermates. In prior studies, when mice were treated with R848 3 times per week for 8 weeks, they displayed severe kidney damage, and 12 weeks of treatment led to a dramatic degree of mortality (Yokogawa et al., 2014). As we wanted to investigate the importance of pathways in production of autoantibodies and cell frequencies in the absence of secondary effects caused by organ failure, we decided to treat mice 3 times weekly for only 4 weeks (**Fig. 1A**).

After 4 weeks of treatment, the Bcl-$6^{flx/flx}$ (Cre-) controls and the Aicda-Cre Bcl-$6^{flx/flx}$ (Cre+) mice showed similar, significant increases in spleen weight upon R848 treatment (**Fig. 1B**). Anti-dsDNA autoantibodies of the IgG2c subtype measured in serum were dramatically elevated upon R848 treatment compared with untreated animals. Surprisingly, there was a trend towards higher levels in treated Cre+ mice compared with treated Cre- mice (**Fig. 1C**). A similar trend towards an increase was seen in total IgG2c levels (**Fig. 1D**). No statistically significant differences in total IgG1 and total IgG3 levels were seen upon treatment (**Fig. 1E and F**).

To validate the effect of R848 treatment and the integrity of the GC block in Cre+ mice, we carried out immunofluorescence staining of spleens to identify GC formation (**Fig. 1G-J**). Using the proliferation marker Ki67 and the naïve B cell marker IgD, it was evident that larger and more frequent GCs were observed upon R848 treatment in Cre- animals (**Fig. 1G, H and K**). Quantification revealed that this difference was statistically significant (**Fig. 1L**). Cre+ animals did not display any baseline or R848-induced GCs (**Fig. 1I and J**). However, in Cre+ treated mice we did observe many proliferating cells at the T-B border and in the red pulp (**Fig. 1J**), likely abortive primary foci and extrafollicular foci, respectively.

Flow cytometric analyses of inguinal LNs (IngLNs), mesenteric LNs (MesLN), and the spleen were carried out (**Fig. 1M-Q, Fig S1A**). In treated animals, we saw slight increases in monocyte and neutrophil frequencies in some of the tissues (**Fig. 1M and N**), and a slight increase in B cell frequencies in the skin-draining IngLNs (**Fig. 1O**), which might be caused by the direct stimulatory effect from the R848 treatment of the ear skin. We observed robust GC B cell frequencies in Cre- R848 treated mice, compared to untreated littermates (**Fig. 1P**). No GC B cells were found in Cre+ animals, further validating the fidelity of the GC block (**Fig. 1P**). Surprisingly, despite this, we found a significant increase in PB/PC frequencies upon

423 treatment in both groups, and the level was significantly higher in the spleens of mice
424 harboring a GC block compared to Cre- R848-treated littermate controls (**Fig. 1Q**). Splitting
425 up for PB and PC, it was clear that this difference between the two groups for the spleen was
426 attributable to PB (**Fig. S1B**) rather than PC (**Fig. S1C**) expansion in Cre+ animals, as compared
427 to Cre- littermates. This observation corresponded well with the increase in plasma IgG2c
428 autoantibody levels as well as total IgG2c levels (**Fig 1C and D**). Taken together, this
429 surprisingly indicated an exacerbated autoimmune phenotype in GC block mice compared to
430 GC sufficient mice upon R848 treatment.

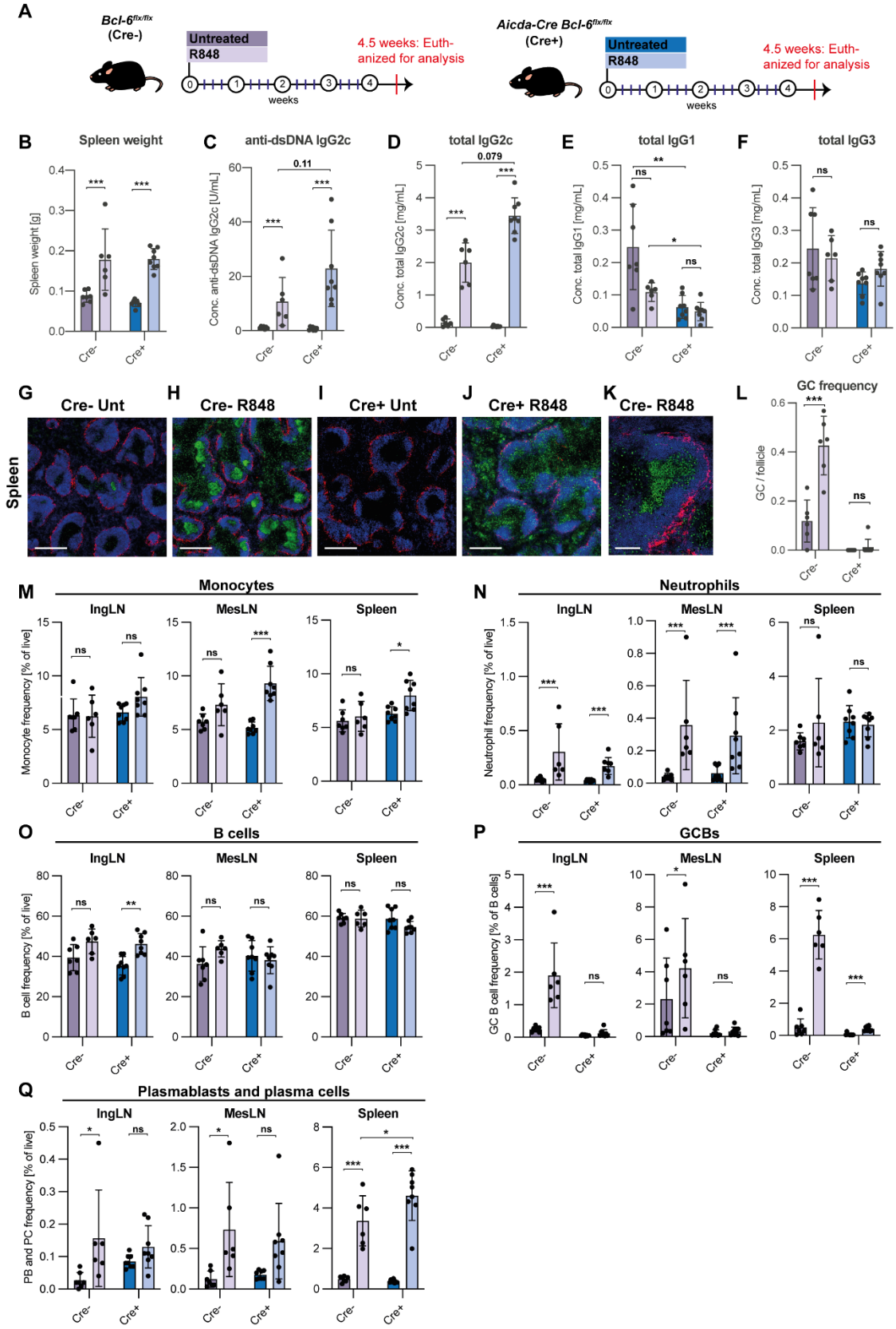


**Figure 1.** GC block causes increased levels of autoantibodies and PB/PCs in SLE-like mice. (**A**) Schematic overview of experimental setup and treatment protocol. Bcl-6$^{flx/flx}$ (Cre-, purple) and Aicda-Cre Bcl-6$^{flx/flx}$ (Cre+, blue) mice were either left untreated (dark color, n = 7 and n = 8, respectively) or treated

with R848 (light color, n = 6 and n= 8, respectively), as indicated. (**B**) Spleen weights. (**C**) Anti-dsDNA IgG2c levels. (**D**) Total IgG2c levels. (**E**) Total IgG1 levels. (**F**) Total IgG3 levels. (**G**) Representative confocal micrograph of spleen from a Cre- untreated animal, stained for CD169 (red), IgD (blue) and Ki67 (green). Scale bar is 400 µm (**H**). As G, but for a Cre- R848-treated animal. (**I**) As G, but for a Cre+ untreated animal. (**J**) As G, but for a Cre+ R848-treated animal. (**K**) High-resolution image of a GC from a Cre- R848-treated mouse. Scale bar is 100 µm. **L**) GC per follicle in spleen. (**M**) Flow cytometry analyses of monocyte frequencies in IngLN, MesLN, and spleen (Ly6CG$^{int}$ of live, singlet leukocytes). (**N**) As M, but neutrophil frequencies (Ly6CG$^{hi}$ of live, singlet leukocytes). (**O**) As M, but B cell frequencies (B220$^{+}$ CD4$^{-}$ CD8$^{-}$ of live, singlet leukocytes). (**P**) As M, but GCB frequencies (CD95$^{hi}$ CD38$^{lo}$ of B cells). (**Q**) As M, but PB and PC frequencies (CD138$^{hi}$ of live, singlet leukocytes). Data are pooled from two independent experiments. Bar graphs show mean ± SD. Two-way ANOVA with Holm-Sidak's post hoc test was used to analyze the data. ns = p≥0.05, * = p<0.05, ** = p<0.01, *** = p<0.001.

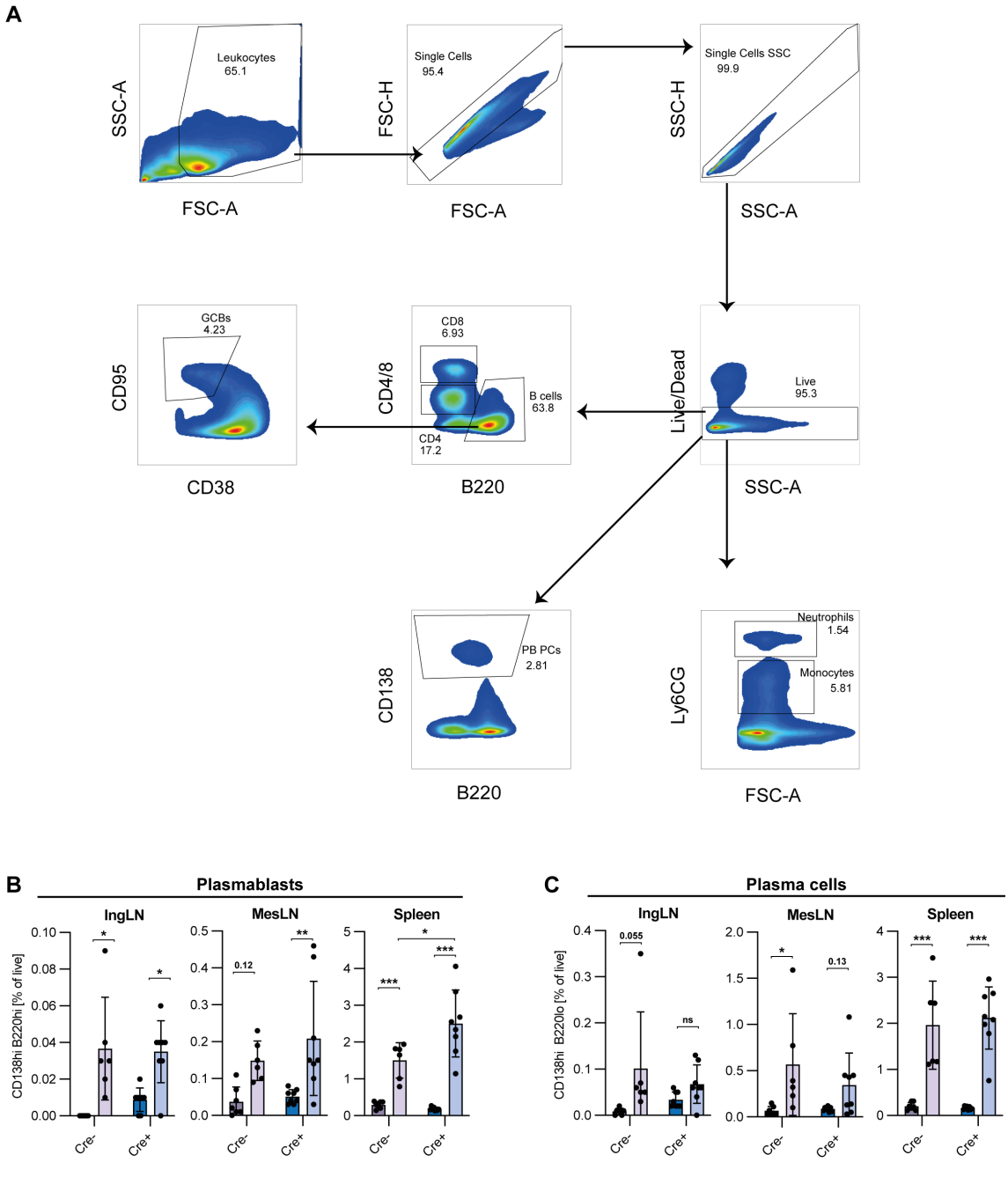

451 **Supplementary Figure 1.** Gating strategy for R848 cohorts, PB and PC frequencies. (**A**) Leukocytes
452 were gated based on size (FSC-A) and granularity (SSC-A). Doublets were excluded with two singlet
453 gates, first FSC-H vs. FSC-A, and then SSC-H vs. SSC-A. After that, dead cells were excluded. From the
454 live gate, monocytes and neutrophils were gated using the Ly6C/G marker. Moreover, B cells were
455 selected, from which GC B cells were selected based on CD95 expression and the absence of CD38
456 expression. PB and PCs were selected from the live gate based on CD138. (**B**) PB ($CD138^{hi}$ $B220^{hi}$ of
457 live, singlet leukocytes) frequencies across secondary lymphoid tissues. (**C**) PC ($CD138^{hi}$ $B220^{lo}$ of live,
458 singlet leukocytes) frequencies across secondary lymphoid tissues. Data in B and C are pooled from
459 two independent experiments. Bar graphs show mean ± SD. Two-way ANOVA with Holm-Sidak's post
460 hoc test was used to analyze the data. ns = $p \geq 0.05$, * = $p<0.05$, ** = $p<0.01$, *** = $p<0.001$.
461
462
463 To further understand the local effects of R848 treatment, we performed
464 immunofluorescence microscopy analyses of draining auricular lymph nodes (AurLNs) from
465 treated mice and untreated controls. We observed gross enlargement of the lymph nodes of
466 treated animals, with a robust induction of GCs in Cre- R848-treated mice (**Fig. S2A**). In
467 comparison, the Cre+ R848-treated mice had many proliferating cells outside the follicles (**Fig.**
468 **S2A**). These dividing cells in the AurLNs overlapped to some extent with the PC marker CD138,
469 pointing towards dividing extrafollicular PCs (**Fig. S2B**).
470

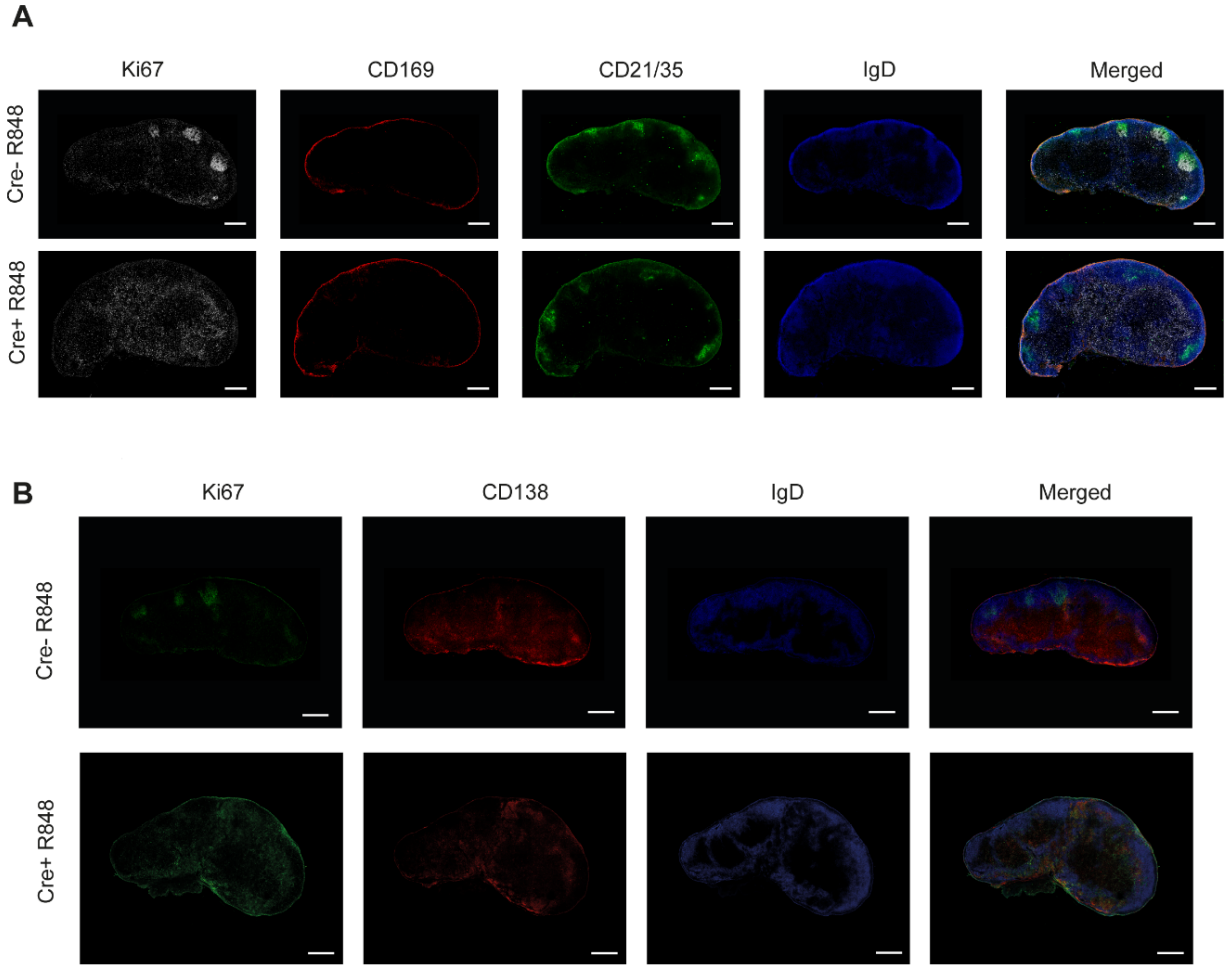


471
472
473 **Supplementary Figure 2.** Immunofluorescence stainings show dividing cells in the paracortex of the
474 AurLN which overlaps with CD138 staining. (**A**) The following targets were stained for: Ki67 (white),

475 CD169 (red), CD21/35 (green), IgD (blue). (**B**) The following targets were stained for: Ki67 (green),
476 CD138 (red), IgD (blue). Scale bar is 350 µm. Images were generated by tile scanning with a 10%
477 overlap using a mechanical stage, followed by stitching. Channel intensities have been adjusted for
478 visual clarity.
479
480
481 **Nanoparticle tracking analyses**
482 Using nanoparticle tracking analyses, we recently identified unique superoligomeric
483 complexes (spMBL) formed between cell-free DNA and mannan-binding lectin (MBL), as a
484 hallmark in blood samples from SLE patients and lupus mice (Juul-Madsen et al., 2021). These
485 spMBL complexes correlated with disease activity in SLE patients, and correlated with
486 formation of GCs and drove loss of immunological tolerance in a murine lupus model (564Igi).
487 To further understand the importance of the increased anti-dsDNA IgG2c autoantibodies in
488 Cre+ R848-treated mice, in the face of a complete absence of GCs, we implemented this
489 nanoparticle tracking approach (**Fig. 2A-C**). We analyzed superoligomeric complexes in the
490 band from 90-130 nm (**Fig. 2D and E**). In agreement with spMBL as a lupus marker, treated
491 mice tended towards higher levels, as compared to untreated mice, but interestingly, we also
492 observed a global trend towards higher levels in Cre+ compared to Cre- animals (**Fig. 2F**).
493 Although they did not reach statistical significance, these observations were well in line with
494 the previously noted increases in anti-dsDNA and total IgG2c antibodies upon R848
495 treatment, and in Cre+ compared to Cre- animals (**Fig. 1C**).
496
497 In our prior study on autoimmune mice carrying an autoreactive B cell receptor knock-in
498 (564Igi) on a wild-type background (Juul-Madsen et al., 2021), a significant inverse correlation
499 was found between the frequency of splenic GC B cells and the ratio between the spMBL and
500 anti-dsDNA antibody concentrations measured in serum. This suggested that an excess of
501 spMBL increased GC B cell formation while an excess of anti-dsDNA antibodies decreased GC
502 B cell proliferation, or vice versa, indicating a potential negative feedback loop. In
503 consideration of this, we next asked whether the same correlation could be established in the
504 R848 model, and how this phenomenon was impacted in GC block mice.
505
506 In Cre- treated mice, GC B cell frequencies were positively correlated with the concentration
507 of spMBL particles in serum (**Fig. 2G**). Total IgG2c levels were similar between treated Cre+
508 and Cre- mice (**Fig. 2H**) with a significant positive correlation between anti-dsDNA IgG2c and
509 the level of spMBL particles (**Fig. 2I**). A significant positive correlation was also observed
510 between the frequency of splenic GC B cells and the ratio between the spMBL and total IgG2c
511 levels in serum (**Fig. 2J**). Conversely, a significant inverse correlation was found between the
512 frequency of splenic GC B cells and the ratio between the spMBL and anti-dsDNA IgG2c
513 antibody concentrations measured in serum (**Fig. 2K**). Taken together, these findings now
514 took our original observations from the autoreactive B cell receptor knock-in model (564Igi)
515 into the epicutaneous R848 model on wild-type (Cre-) background. Importantly, in Cre+ mice,
516 there was an uncoupling of the concentration of spMBL particles and GC B cell levels,
517 indicating that the GC block failed to curb the production of spMBL complexes.

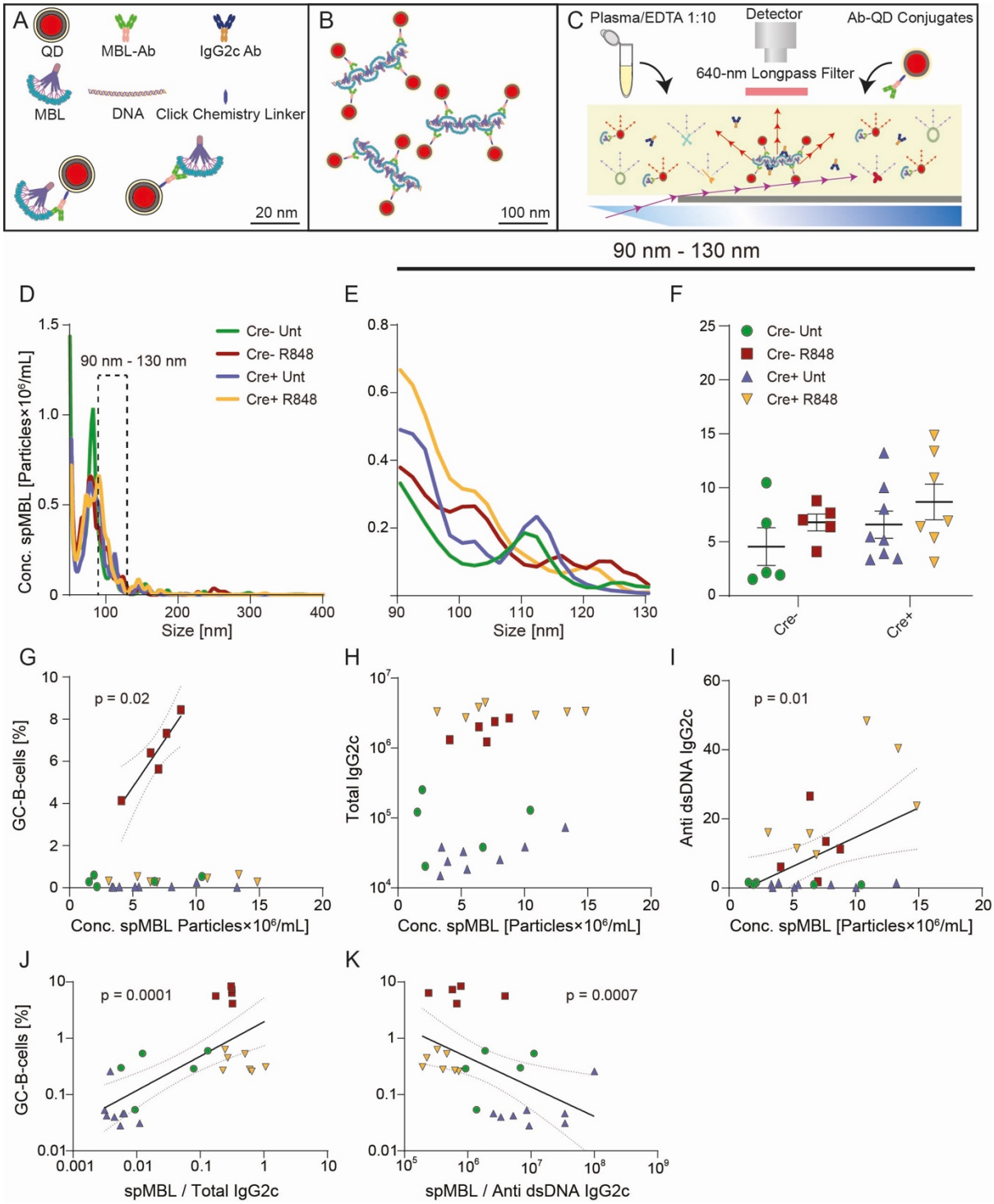


**Figure 2.** Trend towards increased levels of spMBL particles in serum from Cre+ R848 treated mice, and GC and autoantibody correlations with spMBL. (**A-C**) Schematic overview of experimental setup for spMBL analysis of serum samples. (**D**) Samples were tested for the size interval 90-130 nm from Aicda-Cre Bcl-6$^{flx/flx}$ (Untreated: blue, R848-treated: yellow) and Bcl-6$^{flx/flx}$ littermate controls (Untreated: green, R848-treated: red). (**E**) Zoom onto the range of 90 to 130 nm. (**F**) Graph showing mean $\pm$ SEM and individual measurements across treatment protocols for Cre- untreated (n= 5), Cre- R848-treated (n=5), Cre+ untreated (n=8), and Cre+ R848-treated (n=7) mice. (**G**) Correlation analysis of GCB vs. Conc. spMBL. (**H**) Correlation analysis of total IgG2c levels vs. Conc. spMBL. (**I**) Correlation analysis of anti-dsDNA IgG2c vs. Conc. spMBL. (**J**) Correlation analysis of GCB cells vs. spMBL/total IgG2c (**K**) Correlation analysis of GCB vs. spMBL/anti-dsDNA IgG2c. Two-way ANOVA with Holm-Sidak's

530 post hoc test was used to analyze the data in F. Linear regression models were used to analyze G-K.
531 ns = p≥0.05, * = p<0.05, ** = p<0.01, *** = p<0.001.
532
533
534 **Enhanced immune complex deposition in kidneys of R848-treated mice**
535 To understand the pathological importance of the GC block in R848-treated mice and the
536 elevated serum IgG2c, serum anti-dsDNA IgG2c and spMBL levels, we investigated whether
537 there were any pathological changes associated with lupus nephritis in the kidneys. First, we
538 carried out Periodic acid-Schiff (PAS) staining, which displayed no obvious kidney injury upon
539 R848 treatment (**Fig. 3A**). Apart from the presence of mesangial and capillary immune
540 deposits, histopathological changes associated with lupus nephritis may include increased
541 matrix or mesangial cellularity, endocapillary proliferation, thickening of capillary walls,
542 glomerular tuft necrosis, extracapillary proliferation (crescents), karyorrhexis, hyaline
543 thrombi (micronodular intracapillary aggregation of immune complexes), and glomerular
544 sclerosis (segmental or global), as well as, rarely, pathognomonic hematoxylin bodies
545 (Gasparotto et al., 2020; Weening et al., 2004). However, no significant histopathologic
546 findings were identified by light microscopy in any of the mice included in any of the groups.
547 In line with the PAS stainings, we did not observe any differences in glomerular nephrin levels
548 among the groups, suggesting normal glomerular podocytes (**Fig. 3B**). As we could not identify
549 any gross pathological changes nor changes in nephrin levels in the kidneys upon treatment,
550 this verified our short-term treatment strategy in terms of the goal to investigate early
551 immune-driven events in the absence of any secondary pathology.
552
553 To evaluate if immune complex deposition occurred in the kidney glomeruli, and if there were
554 any differences between GC-sufficient and deficient groups, we performed
555 immunofluorescence staining of kidney sections targeting total Ig, C3, and IgG2c (**Fig 3B, 3C,**
556 **3E-G**). The total Ig levels in glomeruli were clearly increased upon R848-treatment.
557 Interestingly, we found a trend towards an increase in the total Ig levels of Cre+ mice
558 compared with littermate R848-treated controls (**Fig. 3B and E**). We also found that there was
559 a significant increase of antibodies of the pathogenic subtype IgG2c upon R848 treatment
560 (**Fig. 3C and G**), and a trend towards an increase in C3 deposition upon R848-treatment (**Fig.**
561 **3C and F**). However, differences between Cre+ and Cre- R848-treated groups were seen
562 neither in C3 nor IgG2c levels (**Fig. 3F and G**).
563
564 Taken together, R848-treated mice displayed immune complex deposition in glomeruli, based
565 on an increased level of C3, total Ig and IgG2c (**Fig. 3E-G**). We corroborated these findings by
566 peroxidase-staining, as a corollary to the immunofluorescence microscopy, and this
567 confirmed the glomerular changes in total Ig, C3 and IgG2c upon R848-treatment (**Fig S3**).
568 Based on the immunofluorescence and immunoperoxidase findings of immune complex
569 deposition (Ig, IgG2c and C3), in the absence of gross histopathological changes of the kidneys,
570 this corresponds to Class I pathology (minimal mesangial lupus nephritis) displaying mesangial
571 immune deposits without mesangial hypercellularity, as defined by the International Society
572 of Nephrology (ISN) and the Renal Pathology Society (RPS) 2004 classification system
573 (Weening et al., 2004).

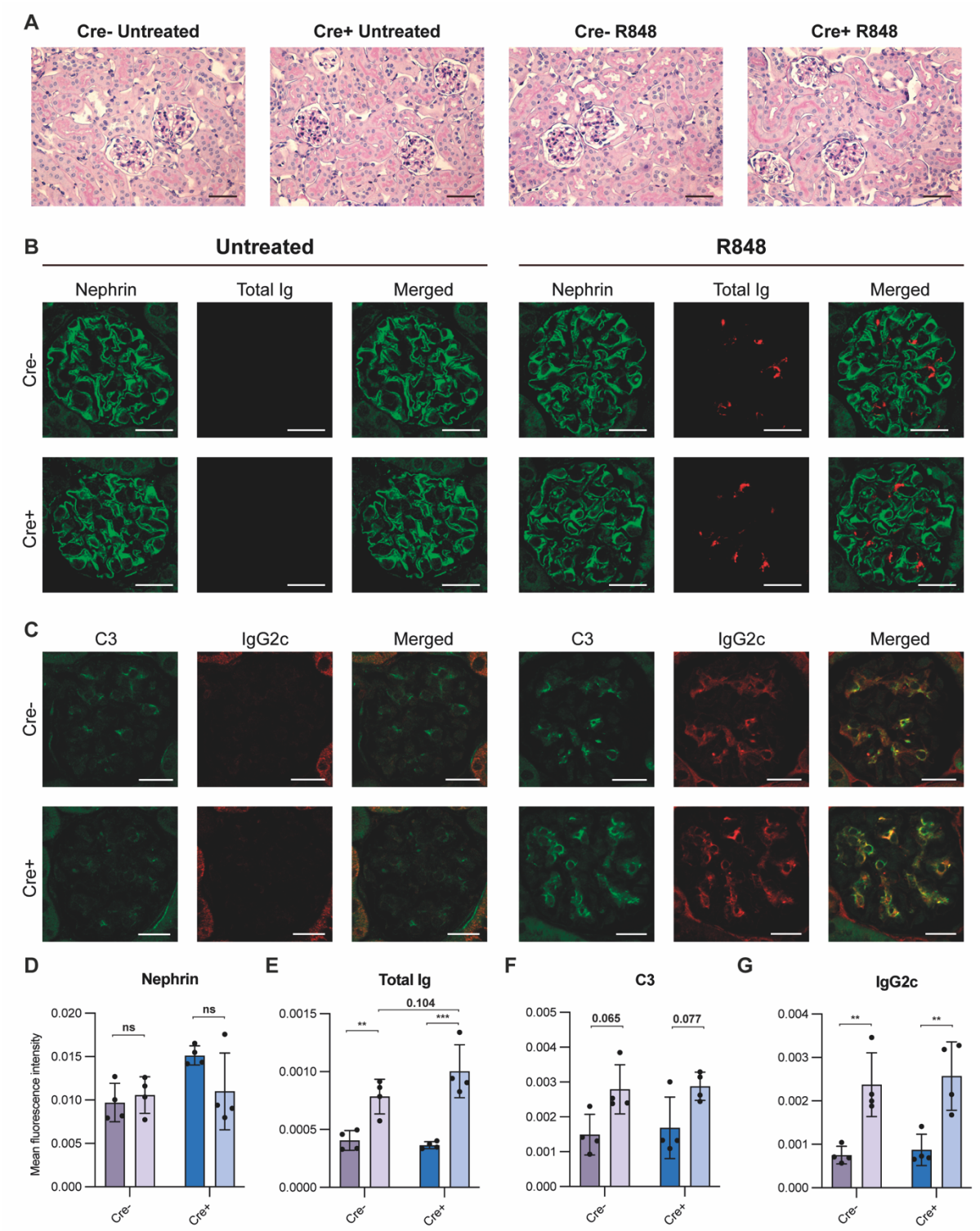


**Figure 3.** Kidney staining reveals immune complex deposition in R848-treated mice. (**A**) PAS stained kidney sections of Cre- untreated (n=4), Cre- R848-treated (n=4), Cre+ untreated (n=4), Cre+ R848-treated (n=4). Scale bar is 50 µm. (**B**) Immunofluorescence staining of kidney sections targeting nephrin (green) and total Ig (red). (**C**) Immunofluorescence staining of kidney sections targeting C3 (green) and IgG2c (red). (**D**) Quantification of immunofluorescence staining targeting nephrin, (**E**) total Ig, (**F**) C3, (**G**) and IgG2c. Scale bar is 20 µm. Two-way ANOVA with Holm-Sidak's post hoc test was used to analyze the data. Bars show mean ± SD. ns = $p>0.05$, * = $p < 0.05$, **= $p<0.01$, *** = $p < 0.001$.

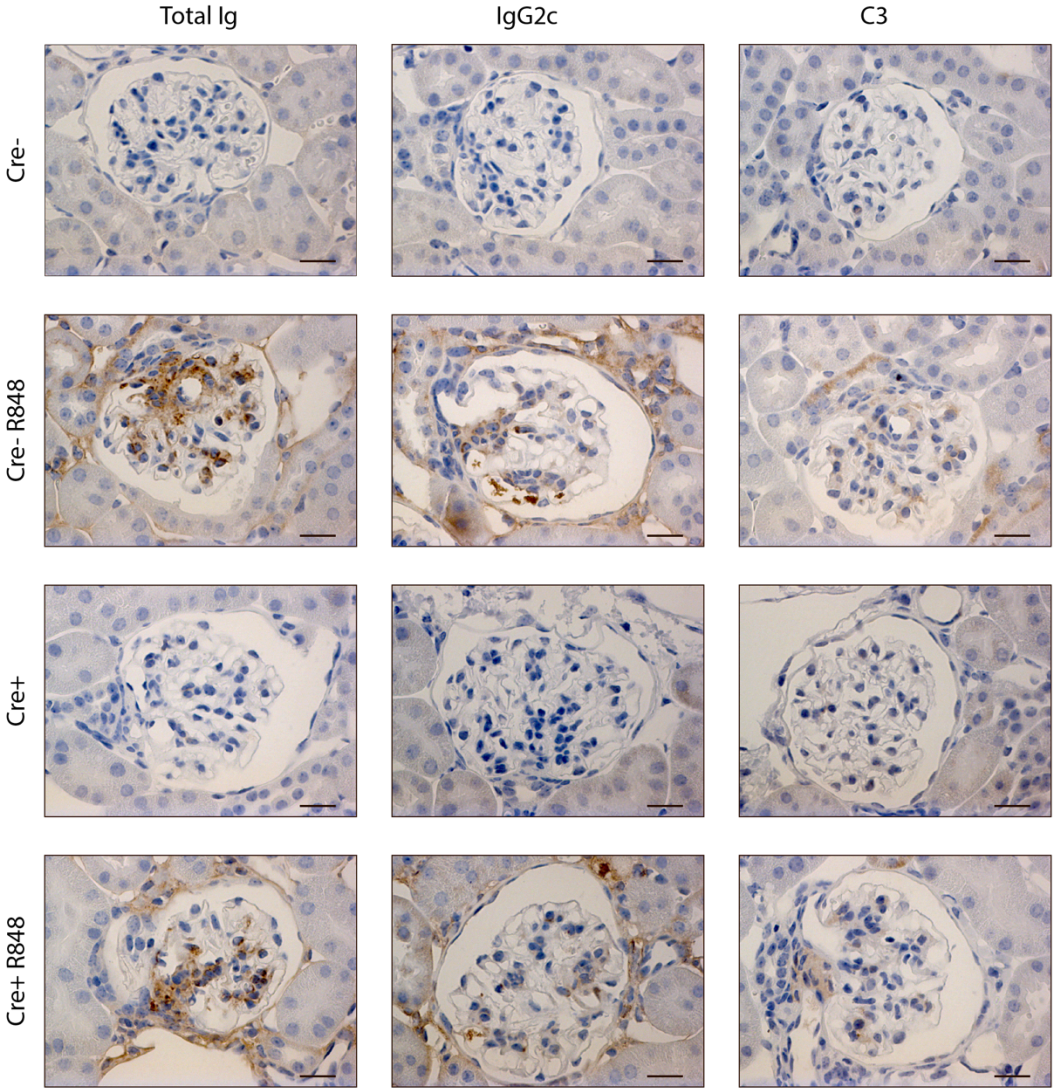


**Supplementary Figure 3.** Increased immune deposits in glomeruli of R848-treated mice. Representative images of immunohistochemical peroxidase staining targeting total Ig, IgG2c and C3 on sections from Cre- untreated (n=4), Cre- R848-treated (n=4), Cre+ untreated (n=4), Cre+ R848-treated (n=4) mice. Scale bars = 20 µm.

**An intrinsic GC block drives B cell differentiation into terminally differentiated PCs**

To investigate whether a B cell intrinsic block of the GC pathway affects their capacity to differentiate into PBs and PCs, we leveraged a modified *in vitro* setup for induced GC B cell (iGB) cultures (Kuraoka et al., 2016; Nojima et al., 2011) (**Fig. 4A**). Naïve B cells purified from Cre- and Cre+ Bcl-6$^{flx/flx}$ mice by negative magnetic-activated cell sorting were seeded onto fibroblast feeder cells expressing CD40L, IL-21 and BAFF, and stimulated with IL-4 (**Fig. 4A**).

The combination of CD40L, BAFF, IL-21, and IL-4 stimulation has previously been shown to induce a robust expansion of B cells with a GC-like phenotype, followed by differentiation of the cells into PBs and finally PCs (Kuraoka et al., 2016; Nojima et al., 2011). Following stimulation of cultures with IL-4, we performed flow cytometric analyses and observed significantly higher B cell (B220+, CD138neg) frequencies in cultures derived from Cre- mice,

604 compared to those derived from Cre+ mice (**Fig. 4B+E and Fig. S4A+B**). This was mirrored by
605 a similar relative increase in PBs (B220+, CD138+) in Cre- cultures (**Fig. 4B and D**), but a relative
606 decrease in PCs (B220neg, CD138+) (**Fig. 4B and C**). Of interest, the total number of cells in
607 the live gate for Cre- cultures was approximately 4 times higher than that of Cre+ cultures
608 (Cre-: 140,000 vs. Cre+: 33,000, **Fig. S4C**). To understand this difference in cell numbers, we
609 investigated whether the Cre+, and hence Bcl-6 deficient, B cells had an increased propensity
610 to undergo apoptosis, because Bcl-6 has previously been reported to suppress P53 and inhibit
611 apoptosis in GC B cells (Phan and Dalla-Favera, 2004). Somewhat surprisingly, we found that
612 upon IL-4 stimulation, there was no difference in the frequency of dead cells (**Fig. 4F and G**),
613 a slight and significant drop in apoptotic cell frequency (**Fig. 4F and H**), and a corresponding
614 increased relative frequency of live cells in Cre+ cultures compared to Cre- cultures on day 6
615 (**Fig. 4F and I**). However, at day 10 there were no significant differences in live, apoptotic, nor
616 necrotic cell frequencies between Cre- and Cre+ cultures (**Fig. 4J-M**). Thus, apoptosis could
617 not account for the dramatic difference in resulting cell numbers between Cre+ and Cre- (**Fig.
618 S4C**). Taken together, this suggested that the higher overall cell numbers in Cre- cultures was
619 not simply a reflection of increased apoptosis among Bcl-6 deficient cells in Cre+ cultures, but
620 rather represented an improved intrinsic proliferative potential of the Bcl-6 sufficient cells.
621
622 In summary, our iGB experiments revealed a vigorous expansion of B cells and PCs in Cre-
623 cultures, but less pronounced PC differentiation, whereas Cre+ cultures conversely displayed
624 a lesser degree of proliferation but more pronounced PC differentiation. This suggested that
625 B cells with an intrinsic GC block may differentiate quicker to PCs, and thereby lose their
626 proliferative capacity, a notion that is in line with the established function of Bcl-6 in
627 repressing upregulation of Blimp-1 (Vasanwala et al., 2002).

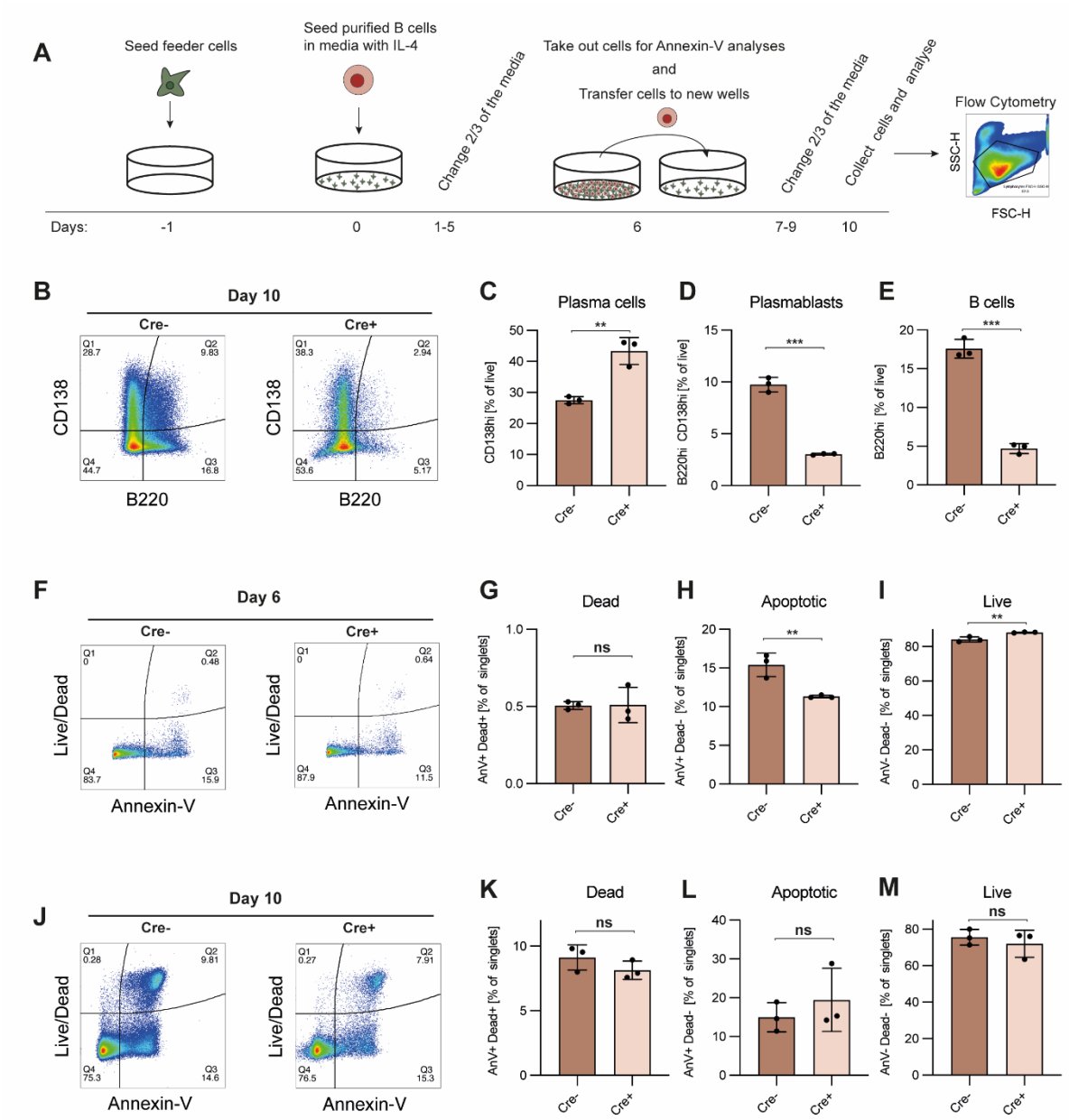


**Figure 4.** Bcl-6 deficient cells more readily differentiate into PCs in iGB cultures. B cells in iGB cultures were treated with IL-4 in conjunction with CD40L, BAFF, and IL-21. (**A**) Schematic overview of the iGB culture system. (**B**) Representative terminal CD138 vs. B220 bivariate plot for iGB cultured B cells stimulated with IL-4. (**C**) Bar graph showing B cell frequencies (B220+, CD138neg). (**D**) As C, but showing PB frequencies (B220+, CD138+). (**E**) As for C, but showing PC frequencies (B220neg, CD138+). Data are representative of three independent experiments with a cumulative 8 replicates in total. Bar graphs show mean ± SD. (**F**) Day 6 representative terminal Live/Dead vs. Annexin V bivariate plot for iGB cultured B cells stimulated with IL-4. (**G**) Bar graph showing dead cell frequencies (AnV-, Dead+). (**H**) As F, but showing apoptotic cell frequencies (AnV+, Dead-). (**I**) As for F, but showing live cell frequencies (AnV-, Dead-). (**J**) Day 10 representative terminal Live/Dead vs. Annexin V bivariate plot for iGB cultured B cells stimulated with IL-4. (**K**) Bar graph showing dead cell frequencies (AnV-, Dead+). (**L**) As for K, but showing apoptotic cell frequencies (AnV+, Dead-). (**M**) As for K, but showing live cell frequencies (AnV-, Dead-). Data for apoptosis assays are from one experiment with 3 replicates. Bar graphs show mean ± SD. Unpaired t-tests were used to analyze all datasets. ns = $p \geq 0.05$, * = $p<0.05$, ** = $p<0.01$, *** = $p<0.001$.

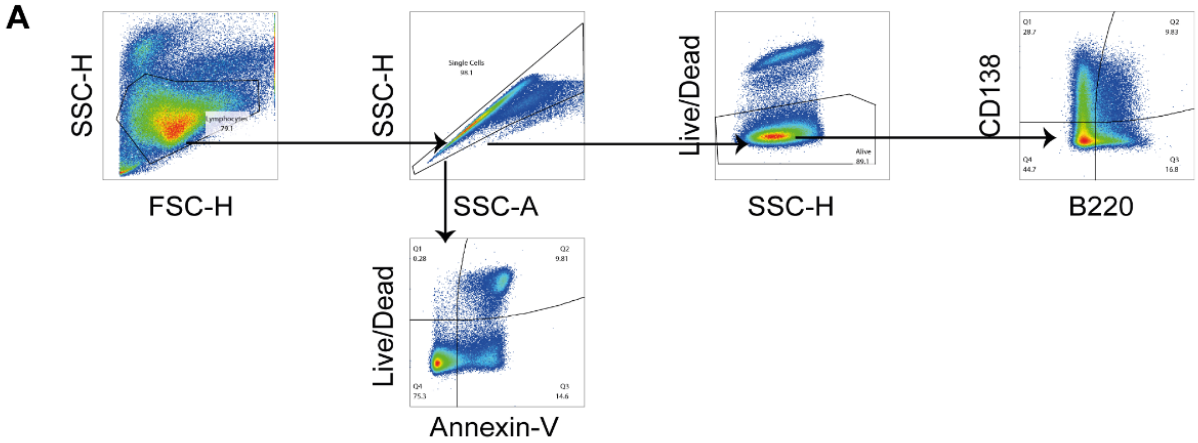


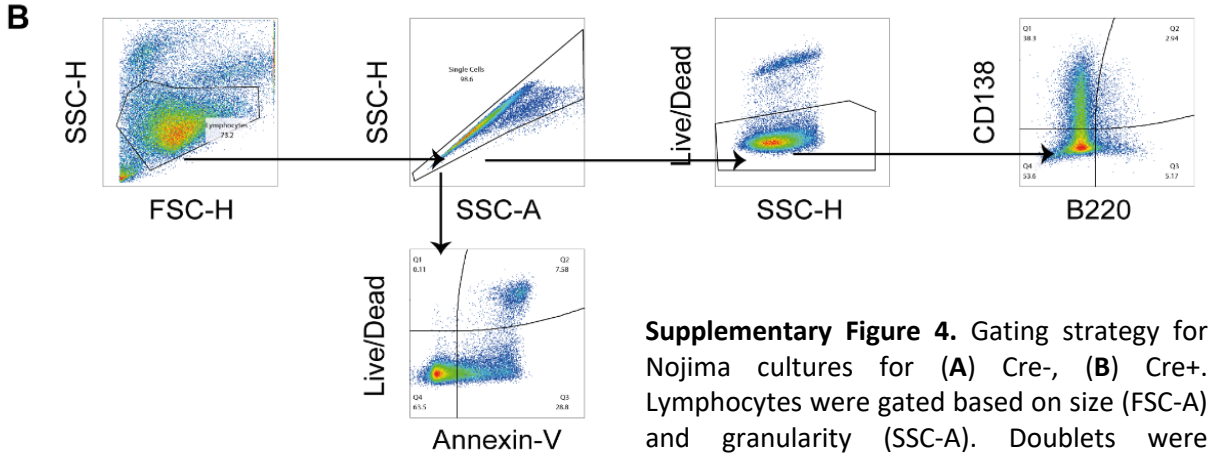


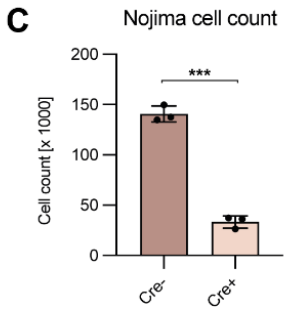


**Supplementary Figure 4.** Gating strategy for Nojima cultures for (**A**) Cre-, (**B**) Cre+. Lymphocytes were gated based on size (FSC-A) and granularity (SSC-A). Doublets were excluded with a singlet gate (SSC-H vs. SSC-A). Apoptotic cells were gated based on the singlet gate using Annexin V and live/dead marker. Dead cells were excluded, and PCs, PBs and B cells were gated based on CD138 and B220 levels. (**C**) Live cell count from flow cytometry on day 10. Bar graph shows mean ± SD. ns = p≥0.05, * = p<0.05, **= p<0.01, *** = p<0.001.

**B cells harboring a GC block competitively contribute to the PC compartment in an autoreactive setting**

Our observation that Bcl-6 deficient B cells rapidly lost their replicative potential *in vitro* (**Fig. 4**) was somewhat at odds with our *in vivo* observations from the R848 model, which displayed a global increase in PCs and autoantibodies (**Fig. 1**). This is because even if Bcl-6 deficient cells more readily became PCs, their poorer capacity to expand compared to Bcl-6 sufficient cells would be predicted to limit PC output. However, it was possible that the constant autoinflammatory drive in an *in vivo* setting where B cells were globally prevented from differentiating down the GC pathway would dysregulate the PC differentiation process and disproportionately drive extrafollicular differentiation. To address this possibility, we asked whether B cells with a GC block would be precluded from contributing to the PC pool in an environment where a large fraction of competitor B cells could form GCs. To achieve this, we

660 leveraged a mixed bone marrow (BM) chimera model allowing interrogation of the
661 competitive potential of B cells with a defined genetic defect in a lupus-like setting (Degn et
662 al., 2017b; Wittenborn et al., 2021). In this model, an autoreactive B cell receptor knock-in
663 clone (clone 564Igi) initiates an autoreactive process that subsequently recruits proto-
664 autoreactive B cells from the non-564Igi B cell population. The B cells derived from the 564Igi
665 compartment eventually are outcompeted and constitute only a minor fraction of the total B
666 cell repertoire. Uniquely to this model, the spontaneous autoreactive GCs established by the
667 564Igi compartment become populated and chronically self-sustained by the non-564Igi (WT)
668 B cells and gain independence from the initial 564Igi trigger. From around six weeks after
669 reconstitution, GCs are almost exclusively (~95%) composed of WT-derived cells (Degn et al.,
670 2017b; Green et al., 2021). Reconstitution with a third of each of 564Igi BM, BM from a wild-
671 type donor, and BM from a donor harboring a specified genetic defect, hence results in
672 chimeras with two equal-sized compartments of B cells sufficient or deficient in the gene of
673 interest. With the use of appropriate congenic markers, their competitive recruitment and
674 participation in the autoreactive GC reaction and relative contribution to the PC compartment
675 can subsequently be evaluated to elucidate the functional relevance of their intrinsic
676 molecular differences. Accordingly, we set up mixed BM chimeras by irradiating WT CD45.1/1
677 recipients and reconstituting with 1/3 of each of 564Igi knock-in BM, WT CD45.1/1 BM, and
678 either Aicda-Cre+ Bcl-6$^{flx/flx}$ or Aicda-Cre- Bcl-6$^{flx/flx}$ BM (**Fig. 5A and S5**).
679
680 There were no differences in the basic parameters when comparing Cre- control BM chimera
681 mice with Cre+ BM chimera mice, in which approximately 50% of the B cells harbored a GC
682 block (**Fig. 5B-H**). That is, aside from a very small but significant relative increase of CD8 T cells
683 in IngLN of Cre+ chimeras, we saw no statistically significant differences in anti-dsDNA IgG2c
684 (**Fig. 5B**), total anti-dsDNA Ig (**Fig. 5C**), B cell frequencies (**Fig. 5D**), CD4 and CD8 T cell
685 frequencies (**Fig. 5E and F, respectively**), overall GC B cell frequencies (**Fig. 5G**) and PB/PC
686 frequencies (**Fig. 5H**) between the groups. This confirmed that the two groups of chimeras
687 were comparable and had robust GCB and PC compartments. In the total B cell compartment,
688 CD45.2 positive cells were present at levels comparable to that of CD45.1 cells in both Cre-
689 (**Fig. 5I**) and Cre+ (**Fig. 5J**) chimeras. However, within the GC B cell gate, CD45.2 cells were
690 robustly represented in Cre- chimeras, but virtually absent in Cre+ chimeras (**Fig. 5I and J**).
691 When quantifying this effect across chimeras and expressing as the ratio of CD45.2 of GCB
692 relative to CD45.2 of total B cells, it was clear that Bcl-6 deficient cells, as expected from their
693 genetic deficiency, were incapable of contributing to the GC compartment (**Fig. 5K**). However,
694 when similarly comparing PB/PC ratio over B cells, the cells harboring a GC block remained
695 able to contribute to the final PB/PC pool, albeit underrepresented relative to the competitor
696 cells (**Fig. 5L**). Taken together, these findings demonstrated that in a GC-sufficient
697 environment, B cells experiencing a block in their ability to partake in the GC reaction readily
698 contributed to the PB and PC compartments.

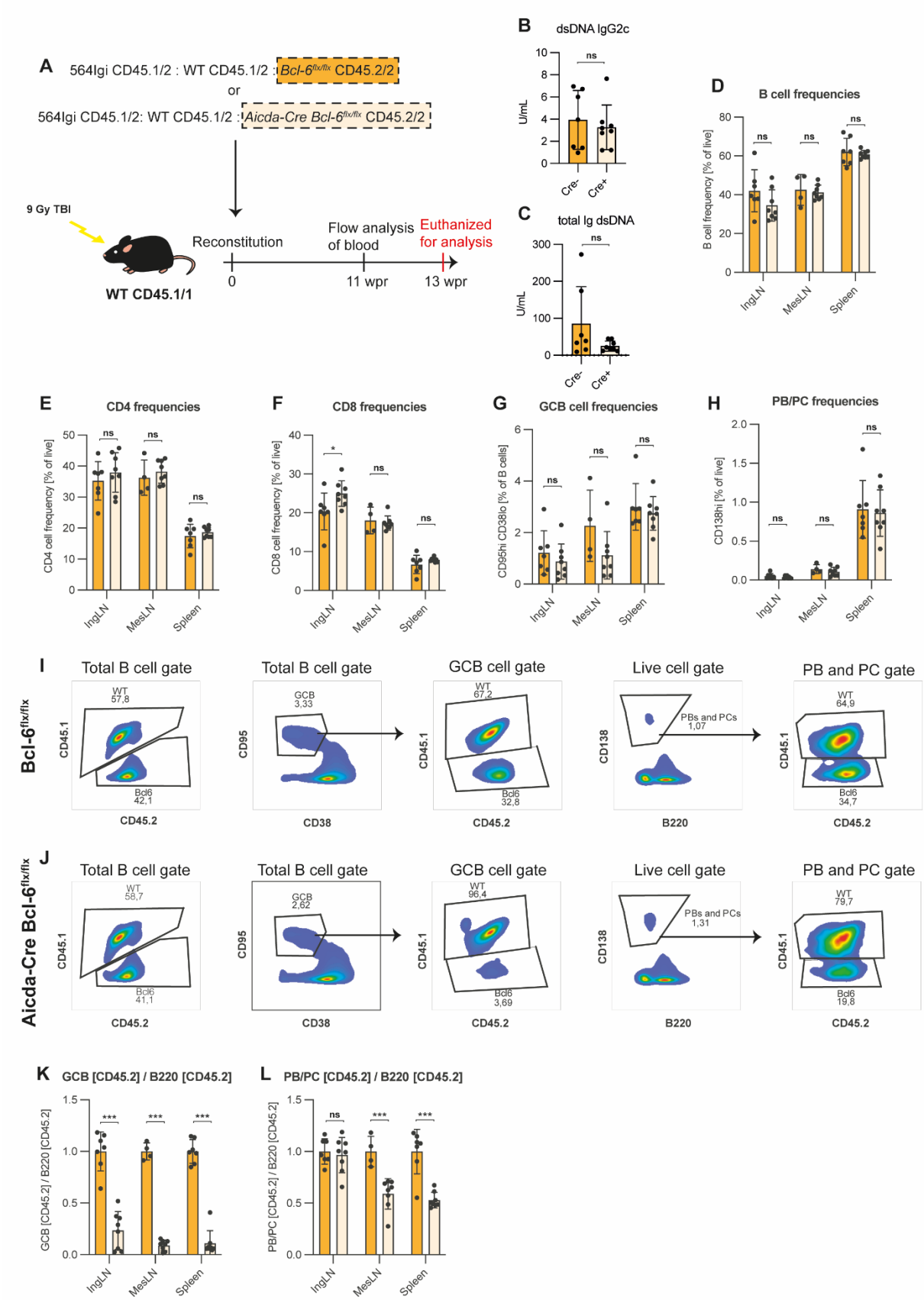


**Figure 5.** B cells harboring a GC block contribute to the PC lineage in a GC sufficient environment. (**A**) Schematic overview of the mixed bone marrow chimera setup. Lethally irradiated CD45.1/1 recipients

were reconstituted with CD45.2/2 564Igi BM, WT CD45.1/2 BM and either Bcl-6$^{flx/flx}$ (Cre-, orange, n = 7) or Aicda-Cre Bcl-6$^{flx/flx}$ (Cre+, light orange, n=8). (**B**) dsDNA IgG2c TRIFMA. (**C**) total Ig TRIFMA. (**D**) Flow cytometric analysis of B cell frequencies (B220$^{+}$ of live, singlets). (**E**) CD4 frequencies (CD4 of live, singlets). (**F**) CD8 frequencies. (**G**) GCB frequencies (CD95$^{hi}$ CD38$^{lo}$ of B cells). (**H**) PB/PC frequencies (CD138$^{hi}$ of live, singlets). (**I**) Representative bivariate plots with gates for Bcl-6$^{flx/flx}$ chimeras. (**J**) Representative bivariate plots with gates for Aicda-Cre Bcl-6$^{flx/flx}$ chimeras. (**K**) Ratio of CD45.2+ of GCB to CD45.2+ of total B cells. (**L**) Ratio of CD45.2+ of PBs/PCs to CD45.2+ of total B cells. The results are obtained from a single experiment with the number of mice given above. Bar graphs show mean ± SD. ns = p≥0.05, * = p<0.05, **= p<0.01, *** = p<0.001.

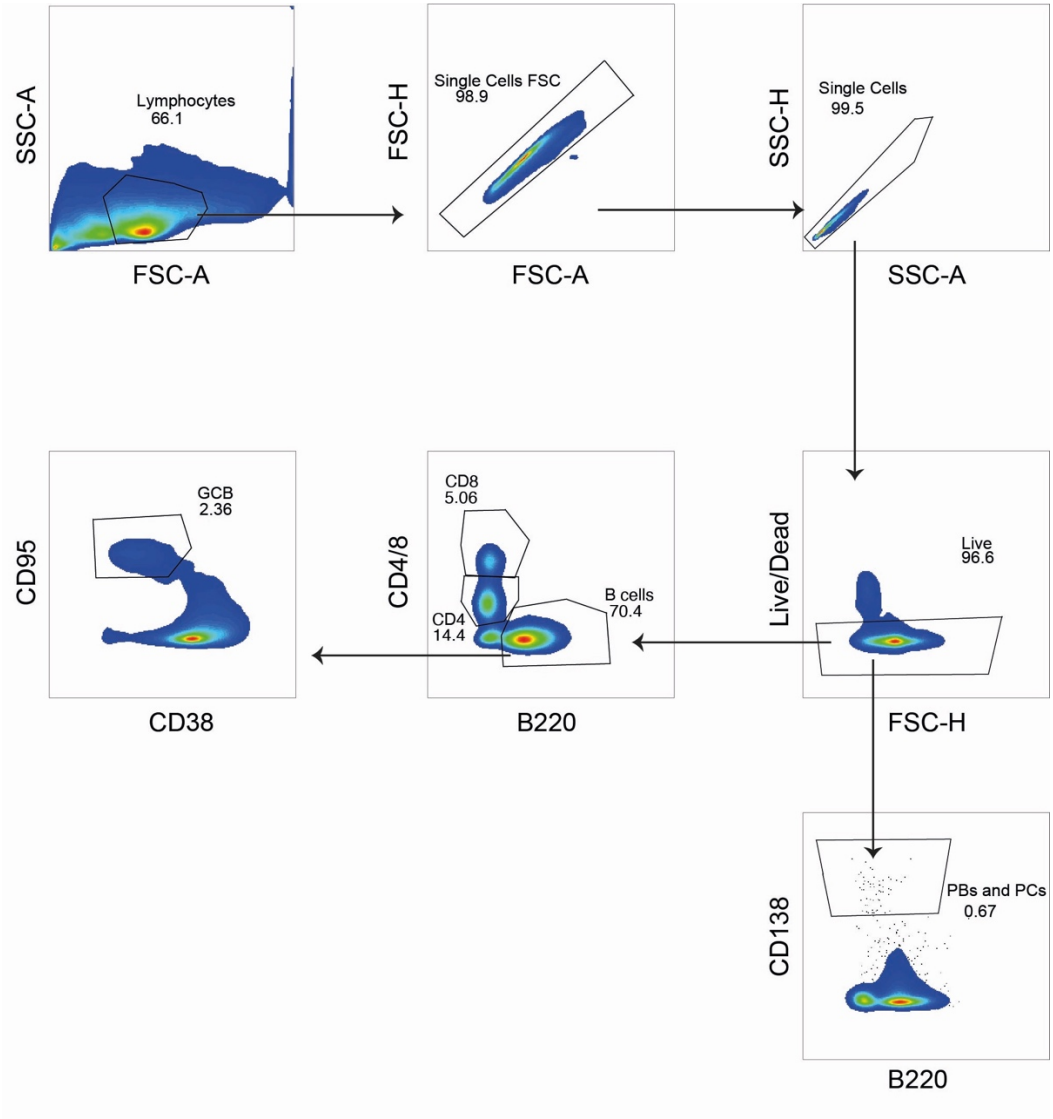


**Supplementary Figure 5.** Gating strategy for the mixed bone-marrow chimera model cohort: Leukocytes were gated based on size (FSC-A) and granularity (SSC-A). Doublets were excluded with two singlet gates, first FSC-H vs FSC-A, and then SSC-H vs. SSC-A. Dead cells were excluded. B cells were selected from the live gate, from which GCBs were selected based on CD95 expression and the absence of CD38 expression. PBs and PCs were selected from the live gate based on CD138 expression.

723 **The extrafollicular pathway is sufficient to drive early hallmarks of autoimmunity in a**
724 **second, independent lupus model**
725 To further evaluate the robustness of our central observation that extrafollicular responses
726 were sufficient to compensate or could even exacerbate autoimmune progression, we set out
727 to test the effect of a complete GC block in a second, independent lupus model, 564Igi. The
728 564Igi model, which we also used as the driver compartment in the mixed chimeras, is a B cell
729 receptor knock-in model, derived from a B cell clone isolated from an autoreactive F1 hybrid
730 cross of Swiss Inbred (SWR) and New Zealand Black (NZB) mice (Berland et al., 2006; Gavalchin
731 et al., 1985). The clone was originally screened for reactivity with ssDNA, but has been found
732 to react more generally with ribonucleic acids and several ribonuclear proteins (Degn et al.,
733 2017b), a polyreactivity likely owing to a high cationic pI in its complementarity determining
734 region (Gavalchin et al., 1987). 564Igi mice present with spontaneous GCs and robust levels
735 of circulating anti-DNA antibodies, but do not develop more severe hallmarks of disease until
736 later in life (at least 9-12 months of age). We crossed the 564Igi line with Aicda-Cre Bcl6$^{flx/flx}$
737 mice, and backcrossed the heavy and light chain, as well as Bcl6$^{flx}$ to homozygosity, retaining
738 hemiparental Aicda-Cre hemizygosity. Hence, Aicda-Cre positive vs. negative offspring, which
739 were invariably 564Igi and Bcl6$^{flx}$ homozygous, could be compared (**Fig. 6A and S6A**). We
740 analyzed this offspring either at adolescence (13-16 weeks) (**Figure 6**) or in early adulthood
741 (17-23 weeks of age) (**Figure S6**). At the earlier time point, the two groups had comparable
742 levels of anti-dsDNA of IgG2a isotype (**Fig. 6B**), whereas GC block 564Igi mice presented with
743 slightly elevated levels of anti-dsDNA IgG2b (**Fig. 6C**), although this difference did not reach
744 statistical significance. Total anti-dsDNA levels were comparable between groups (**Fig. 6D**).
745 Total IgG1 was elevated in GC-sufficient littermates (**Fig. 6E**), whereas total IgG2a (**Fig. 6F**) and
746 IgG3 (**Fig. 6G**) were on par. By flow cytometry (**Fig. S7**), we verified that main lymphocyte
747 subsets were comparable between groups across all tissues (**Fig. 6H-J**). Furthermore, the
748 frequency of idiotype positive cells, i.e., cells carrying the knock-in B cell receptor (identified
749 by staining with the anti-idiotype antibody 9D11) was comparable between groups (**Fig. 6K**).
750 We verified that GCs were indeed efficiently blocked in GC block mice (**Fig. 6L**), but despite
751 this, overall PB/PC frequencies (**Fig. 6M**) and PB frequencies (**Fig. 6N**) across tissues were not
752 different between the two groups. PC frequencies were similar in IngLN and MesLN, and
753 slightly elevated in the spleen of GC block mice (**Fig. 6O**). Thus, overall, the GC block did not
754 prevent any of the autoimmune read-outs. This was also the case at the later time point,
755 where no gross differences were observed (**Fig. S6**).
756
757 Taken together, this demonstrated that the GC block failed to curb the main hallmarks of
758 autoimmunity presented by the 564Igi model, further corroborating our findings from the
759 Resiquimod model.

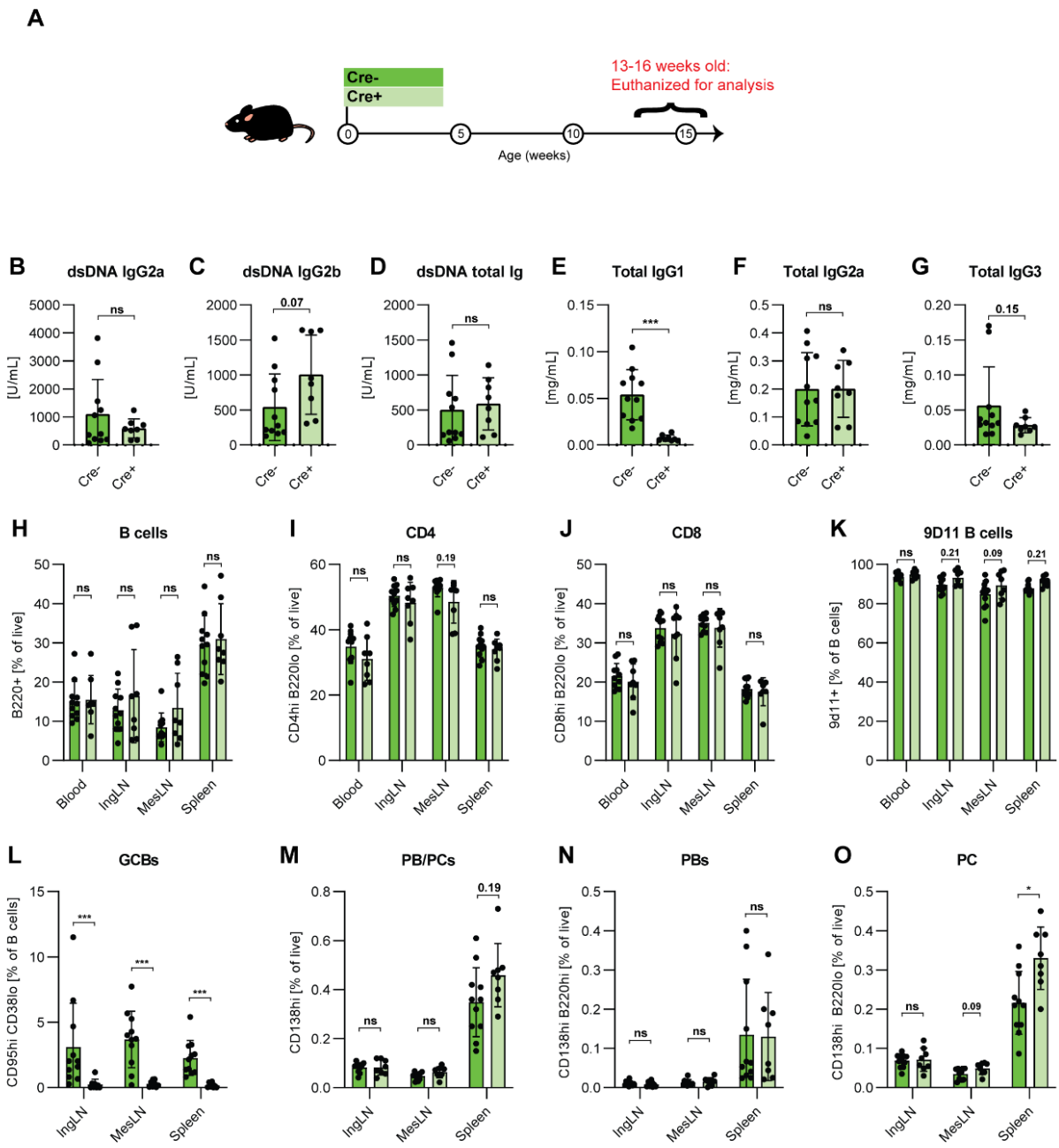


**Figure 6.** GC block causes increased PB/PCs levels in adolescent 564Igi mice. (**A**) Schematic overview of experimental setup: 564Igi-Bcl-6$^{flx/flx}$ (Cre-, dark green) and 564Igi-Aicda-Cre Bcl-6$^{flx/flx}$ (Cre+, light green) mice. (**B**) Anti-dsDNA IgG2a. (**C**) Anti-dsDNA IgG2b. (**D**) Anti-dsDNA total Ig. (**E**) Total IgG1. (**F**) Total IgG2a. (**G**) Total IgG3. Unpaired t-test or Mann-Whitney's test was used was used to analyze TRIFMA data. (**H**) Flow cytometry analyses of B cell frequencies (B220$^{+}$ CD4$^{-}$ CD8$^{-}$ of live, singlet lymphocytes) in blood, IngLN, MesLN, and spleen. (**I**) As H, but CD4 T cells (CD4$^{+}$ B220$^{-}$ of live, singlet lymphocytes). (**J**) As H, but CD8 T cells (CD8$^{+}$ B220$^{-}$ of live, singlet lymphocytes). (**K**) As H, but 9D11 B cell frequencies (9D11$^{+}$ of B cells). (**L**) As H, but GCB frequencies (CD95$^{hi}$ CD38$^{lo}$ of B cells). (**M**) As H, but PB and PC frequencies (CD138$^{hi}$ of live, singlet leukocytes), (**N**) As H, but PC frequencies (CD138$^{hi}$ B220$^{lo}$ of live, singlet lymphocytes), (**O**) As H, but PB frequencies (CD138$^{hi}$ B220$^{hi}$ of live, singlet lymphocytes). Data are pooled from two independent experiments. Bar graphs show mean ± SD. Two-way

ANOVA with Holm-Sidak's post hoc test was used to analyze the data. ns = p≥0.05, * = p<0.05, ** = p<0.01, *** = p<0.001.

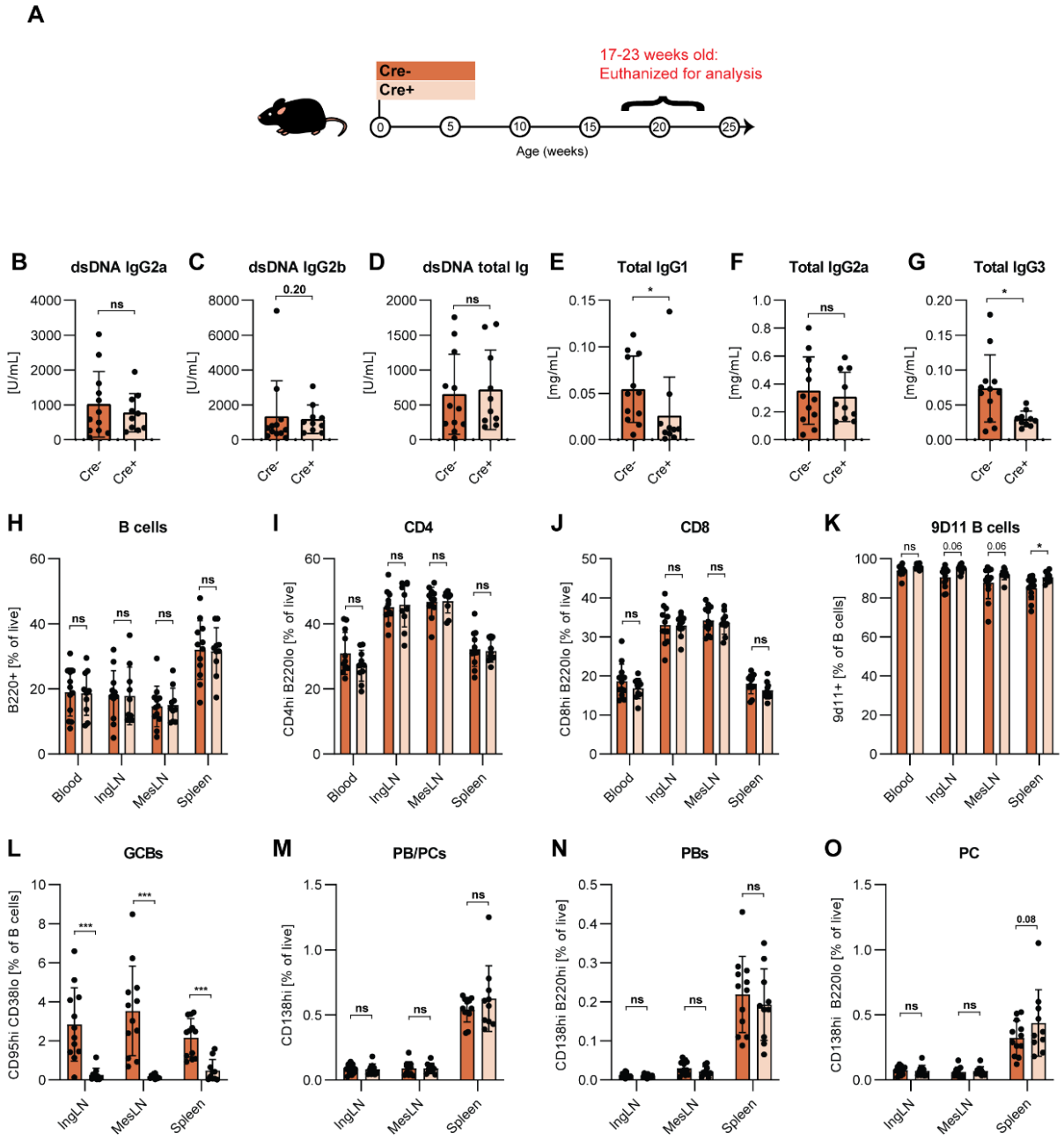


**Figure S6.** GC block does not ameliorate autoimmune phenotype in adult 564Igi mice. (**A**) Schematic overview of experimental setup: 564Igi-Bcl-6$^{flx/flx}$ (Cre-, dark red) and 564Igi-Aicda-Cre Bcl-6$^{flx/flx}$ (Cre+, light red). (**B**) Anti-dsDNA IgG2a. (**C**) Anti-dsDNA IgG2b. (**D**) Anti-dsDNA total Ig. (**E**) Total IgG1. (**F**) Total IgG2a. (**G**) Total IgG3. Unpaired t-test or Mann-Whitney's test was used was used to analyze TRIFMA data. (**H**) Flow cytometry analyses of B cell frequencies (B220$^{+}$ CD4$^{-}$ CD8$^{-}$ of live, singlet lymphocytes) in blood, IngLN, MesLN, and spleen. (**I**) As H, but CD4 T cells (CD4$^{+}$ B220$^{-}$ of live, singlet lymphocytes). (**J**) As H, but CD8 T cells (CD8$^{+}$ B220$^{-}$ of live, singlet lymphocytes). (**K**) As H, but 9D11 B cell frequencies (9D11$^{+}$ of B cells). (**L**) As H, but GCB frequencies (CD95$^{hi}$ CD38$^{lo}$ of B cells). (**M**) As H, but PB and PC frequencies (CD138$^{hi}$ of live, singlet leukocytes), (**N**) As H, but PC frequencies (CD138$^{hi}$ B220$^{lo}$ of live, singlet

789 lymphocytes), (**O**) As H, but PB frequencies (CD138$^{hi}$ B220$^{hi}$ of live, singlet lymphocytes). Data
790 are pooled from two independent experiments. Bar graphs show mean ± SD. Two-way
791 ANOVA with Holm-Sidak's post hoc test was used to analyze the data. ns = p≥0.05, * = p<0.05,
792 ** = p<0.01, *** = p<0.001.
793
794

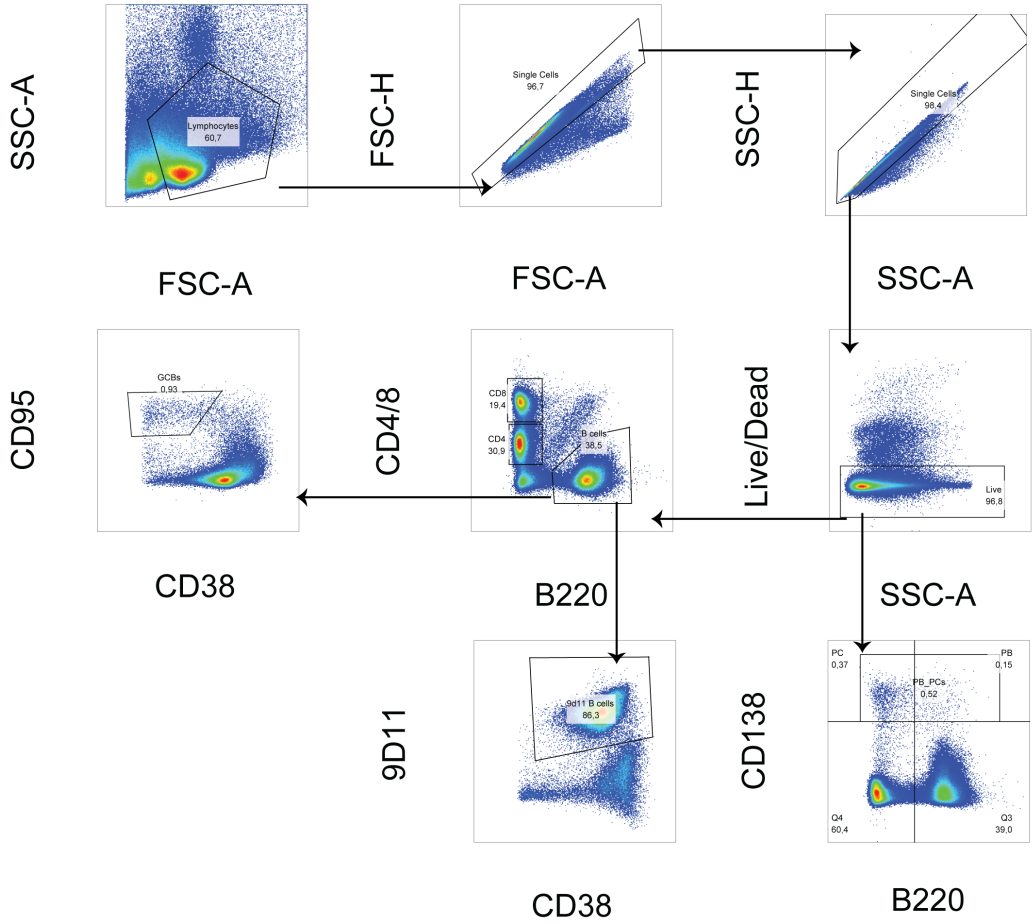


795
796
797 **Supplementary Figure 7.** Gating strategy for the 564Igi model cohort: Lymphocytes were gated based
798 on size (FSC-A) and granularity (SSC-A). Doublets were excluded with two singlet gates, first FSC-H vs
799 FSC-A, and then SSC-H vs. SSC-A. Dead cells were excluded. B cells were selected from the live gate,
800 from which GCBs were selected based on CD95 expression and the absence of CD38 expression.
801 Idiotype (9D11) positive cells were selected from the B cell gate based on 9D11$^{hi}$ expression. PBs and
802 PCs were selected from the live gate based on CD138 and B220 expression.

## Discussion

GCs are believed to be the nexus of autoreactive responses in a range of autoimmune diseases. Due to their role in potent antibody responses, memory generation, and long-lived PC formation, there has been extensive interest in targeting GCs in autoimmune disease. The strategy has proven useful in autoimmune models, but due to off-target effects, did not initially progress through clinical trials (Degn et al., 2017a; Karnell et al., 2019). Considerable efforts have, however, been aimed at circumventing the off-target effects to bring this strategy to market (Espie et al., 2020; Karnell et al., 2019). This notwithstanding, a recent study reported that extrafollicular B cell differentiation into short-lived antibody-forming cells is a key mechanism of anti-DNA autoreactivity (Soni et al., 2020), and it has been argued that more attention should be paid to the non-GC responses, as these may play a critical role in humoral immunity in both mice and men (Jenks et al., 2019).

Here, we took an unbiased approach and asked to what extent a genetic block of GCs would ameliorate autoreactive manifestations in a lupus-like disease model. To our surprise, we found blocking GCs did not lessen autoreactive manifestations, but in some cases worsened these. Upon autoimmune induction, we observed a trend towards an increase in anti-dsDNA antibodies of the IgG2c isotype (**Fig. 1C**) and total IgG2c antibody (**Fig. 1D**) in GC block mice, compared to WT. These changes were also mirrored by a significantly higher frequency of PB/PCs in the spleens of GC block mice, despite a total absence of GCs. In agreement with this, we observed robust deposition of immune complexes in the kidney glomeruli of GC block mice, at least on par with that of GC sufficient controls (**Fig. 3**). This indicated that the extrafollicular pathway could compensate, and in some cases even augment, the autoreactive response. We corroborated this central finding in a second, independent model (**Fig. 6**), confirming that the observed sufficiency of the extrafollicular response was not model-specific.

To understand the B cell intrinsic effect of a GC block, we leveraged an induced GC B cell culture system. It has previously been noted that Bcl-6 expression can inhibit apoptosis in numerous cell types including (GC) B cells (Kumagai et al., 1999; Kurosu et al., 2003; Phan and Dalla-Favera, 2004). Yet, contrary to expectations, GC block B cells did not display a significantly increased propensity to undergo apoptosis (**Fig. 4H and L**), rather, they much more readily underwent terminal differentiation to PCs, and had a dramatically reduced capacity to expand compared to their wild type counterparts (**Fig. 4**). However, this agreed well with the established cross-regulation between Bcl-6 and Blimp-1, the master regulator of the PC fate, also known as Prdm1 (Vasanwala et al., 2002). Although the increased propensity for terminal PC differentiation was, in principle, well in line with our *in vivo* observations, the lack of proliferative capacity was at the same time at odds with the dramatic PC output in the mice harboring a GC block in B cells. This suggested that the PC differentiation process in mice displaying a global GC block in B cells might be dysregulated, potentially as a consequence of absence of GC-derived antibody feedback, as previously suggested for GC B cells (Zhang et al., 2013). To address this possibility, we asked whether B cells with a GC block would be precluded from contributing to the PC pool in a GC sufficient environment. Our findings demonstrated that this was not the case, although the relative contribution of GC block B cells to the PC pool was smaller than that of GC sufficient B cells (**Fig. 5**). However, given their inability to expand in GCs, the magnitude of the contribution of GC block B cells to the PC compartment in direct competition with GC-sufficient B cells was remarkable. In the

850 infectious setting, an early wave of extrafollicular PCs is crucial for the initial antibody
851 response. However, most PCs produced by the extrafollicular response undergo apoptosis
852 within a matter of days, and the global response becomes dominated by GC-derived
853 responses. In the chronic autoreactive setting, however, the continuous fueling of the
854 autoimmune process may continually renew this population.
855
856 We may speculate that the somewhat lower contribution of the extrafollicular PC
857 compartment in the mixed chimera model compared to that of the R848 model could be a
858 consequence of the markedly different time scales of the two experiments: the mixed
859 chimeras were analyzed 13 weeks post reconstitution, whereas the R848 mice were analyzed
860 4.5 weeks after commencement of treatment. This could be important, because at this point
861 it remains unclear whether the GC responses observed in our models contribute a
862 qualitatively different response to the autoimmune progression, e.g., through production of
863 memory B cells and long-lived PCs that may perpetuate and dominate the chronic response
864 over longer periods of time. By extension, the GC pathway may differentially allow epitope
865 spreading and inclusion of alternative antigens over time, as seen in human SLE patients
866 (Arbuckle et al., 2003). At least, it seems plausible that the longer the autoimmune process
867 has persisted, the more the long-lived GC responses and their derived memory output come
868 to dominate the process, and conversely, the short-lived extrafollicular responses may govern
869 the early stages of the response and, as previously suggested, the very early break-of-
870 tolerance driven by nucleic acid-containing antigens (Soni et al., 2020; Sweet et al., 2011).
871 Such considerations notwithstanding, our findings in the second model, 564Igi, analyzed at
872 13-16 and 17-23 weeks of age, suggest that even after a chronic response of 5-6 months in
873 duration, the extrafollicular responses are not outpaced by GCs (**Fig. 6 and S6**).
874
875 Interestingly, due to its more potent nature, The GC reaction is believed to be subject to a
876 much higher level of control, through a continued requirement for linked recognition in
877 successive rounds of diversity generation. Furthermore, a specialized subset of Tregs, $T_{FR}$s,
878 exert a dominant negative level of control on the GC reaction (Fahlquist Hagert and Degn,
879 2020). Hence it may be that the extrafollicular pathway in essence represents an evolutionary
880 'backdoor to autoimmunity', unguarded due to its relative insignificance in terms of high-
881 quality, affinity-matured, and memory-inducing antibody responses. In this context, it is
882 fortunate that current CD40L targeting strategies block both the GC and extrafollicular
883 response. However, we suggest that future efforts should be aimed at further elucidating the
884 relative contributions of the extrafollicular and GC pathways. We may speculate that specific
885 targeting of the extrafollicular pathway would be a superior strategy, as it would
886 preferentially block the low quality and poorly controlled responses driving autoimmune
887 progression, while leaving intact the more stringently controlled and high-quality responses
888 that provide protection against infectious agents. Unfortunately, there is much more limited
889 knowledge regarding the biology of the extrafollicular responses, and no transgenic or
890 pharmacologic strategy allowing specific blockade of this pathway exists, making it difficult to
891 evaluate in animal models.
892
893 In summary, our findings here demonstrate that a complete or partial block of the GC
894 pathway is insufficient to curb autoreactive PC differentiation and might in fact exacerbate
895 the autoimmune progression. The GC commitment is controlled by the expression level of the
896 master transcriptional repressor, Bcl-6 (Robinson et al., 2020), which regulates the GC fates

across GC B cells, $T_{FH}$ cells and $T_{FR}$ cells. Interestingly, in the context of the COVID-19 pandemic, it has been observed that Bcl-6$^+$ GC B cells and Bcl-6$^+$ $T_{FH}$ cells are markedly diminished in SARS-CoV-2 infection (Kaneko et al., 2020). It has also been found that critically ill SARS-CoV-2 patients display hallmarks of extrafollicular B cell activation and shared B cell repertoire features previously described in autoimmune settings (Knight et al., 2021; Woodruff et al., 2020). This further highlights the potential link between aberrant extrafollicular responses and autoimmune manifestations.

## Conflict of Interest statement

TV-J and KJ-M are inventors on a submitted patent application (PCT/EP2020/082837), owned by Aarhus University, related to human spMBL as a biomarker for SLE. All other authors declare that the research was conducted in the absence of any commercial or financial relationships that could be construed as a potential conflict of interest.

## Acknowledgements

We thank Hanne Sidelmann for her contributions to immunofluorescence and immunohistochemical staining of kidneys. We would like to acknowledge the AU FACS Core facility for their support and feedback on data related to flow cytometry. We also thank the BioImaging Core at Health for support with microscopy.

## Funding

This project was funded by the Novo Nordisk Foundation (NNF19OC0058454) and the Independent Research Fund Denmark through a *Sapere Aude* Research Leader grant to SED (9060-00038B).

## References


Akkaya, M., B. Akkaya, A.S. Kim, P. Miozzo, H. Sohn, M. Pena, A.S. Roesler, B.P. Theall, T. Henke, J. Kabat, J. Lu, D.W. Dorward, E. Dahlstrom, J. Skinner, L.H. Miller, and S.K. Pierce. 2018. Toll-like receptor 9 antagonizes antibody affinity maturation. *Nat Immunol* 19:255-266.

Arbuckle, M.R., M.T. McClain, M.V. Rubertone, R.H. Scofield, G.J. Dennis, J.A. James, and J.B. Harley. 2003. Development of autoantibodies before the clinical onset of systemic lupus erythematosus. *N Engl J Med* 349:1526-1533.

Berland, R., L. Fernandez, E. Kari, J.H. Han, I. Lomakin, S. Akira, H.H. Wortis, J.F. Kearney, A.A. Ucci, and T. Imanishi-Kari. 2006. Toll-like receptor 7-dependent loss of B cell tolerance in pathogenic autoantibody knockin mice. *Immunity* 25:429-440.

Cornaby, C., L. Gibbons, V. Mayhew, C.S. Sloan, A. Welling, and B.D. Poole. 2015. B cell epitope spreading: mechanisms and contribution to autoimmune diseases. *Immunol Lett* 163:56-68.

Degn, S.E., C.E. van der Poel, and M.C. Carroll. 2017a. Targeting autoreactive germinal centers to curb autoimmunity. *Oncotarget* 8:90624-90625.

Degn, S.E., C.E. van der Poel, D.J. Firl, B. Ayoglu, F.A. Al Qureshah, G. Bajic, L. Mesin, C.A. Reynaud, J.C. Weill, P.J. Utz, G.D. Victora, and M.C. Carroll. 2017b. Clonal Evolution of Autoreactive Germinal Centers. *Cell* 170:913-926 e919.

Domeier, P.P., S.L. Schell, and Z.S. Rahman. 2017. Spontaneous germinal centers and autoimmunity. *Autoimmunity* 50:4-18.

Elsner, R.A., and M.J. Shlomchik. 2020. Germinal Center and Extrafollicular B Cell Responses in Vaccination, Immunity, and Autoimmunity. *Immunity* 53:1136-1150.

Espie, P., Y. He, P. Koo, D. Sickert, C. Dupuy, E. Chokote, R. Schuler, H. Mergentaler, J. Ristov, J. Milojevic, A. Verles, A. Groenewegen, A. Auger, A. Avrameas, M. Rotte, L. Colin, C.S. Tomek, M. Hernandez-Illas, J.S. Rush, and P. Gergely. 2020. First-in-human clinical trial to assess pharmacokinetics, pharmacodynamics, safety, and tolerability of iscalimab, an anti-CD40 monoclonal antibody. *Am J Transplant* 20:463-473.

Fahlquist Hagert, C., and S.E. Degn. 2020. T follicular regulatory cells: Guardians of the germinal centre? *Scand J Immunol* 92:e12942.

Gasparotto, M., M. Gatto, V. Binda, A. Doria, and G. Moroni. 2020. Lupus nephritis: clinical presentations and outcomes in the 21st century. *Rheumatology (Oxford)* 59:v39-v51.

Gavalchin, J., J.A. Nicklas, J.W. Eastcott, M.P. Madaio, B.D. Stollar, R.S. Schwartz, and S.K. Datta. 1985. Lupus prone (SWR x NZB)F1 mice produce potentially nephritogenic autoantibodies inherited from the normal SWR parent. *J Immunol* 134:885-894.

Gavalchin, J., R.A. Seder, and S.K. Datta. 1987. The NZB X SWR model of lupus nephritis. I. Cross-reactive idiotypes of monoclonal anti-DNA antibodies in relation to antigenic specificity, charge, and allotype. Identification of interconnected idiotype families inherited from the normal SWR and the autoimmune NZB parents. *J Immunol* 138:128-137.

Green, K., T.R. Wittenborn, C. Fahlquist-Hagert, E. Terczynska-Dyla, N. van Campen, L. Jensen, L. Reinert, R. Hartmann, S.R. Paludan, and S.E. Degn. 2021. B Cell Intrinsic STING Signaling Is Not Required for Autoreactive Germinal Center Participation. *Front Immunol* 12:782558.

969 Hollister, K., S. Kusam, H. Wu, N. Clegg, A. Mondal, D.V. Sawant, and A.L. Dent. 2013. Insights
970 into the role of Bcl6 in follicular Th cells using a new conditional mutant mouse model.
971 *J Immunol* 191:3705-3711.
972 Jenks, S.A., K.S. Cashman, M.C. Woodruff, F.E. Lee, and I. Sanz. 2019. Extrafollicular responses
973 in humans and SLE. *Immunol Rev* 288:136-148.
974 Juul-Madsen, K., A. Troldborg, T.R. Wittenborn, M.G. Axelsen, H. Zhao, L.H. Klausen, S. Luecke,
975 S.R. Paludan, K. Stengaard-Pedersen, M. Dong, H.J. Moller, S. Thiel, H. Jensen, P.
976 Schuck, D.S. Sutherland, S.E. Degn, and T. Vorup-Jensen. 2021. Characterization of
977 DNA-protein complexes by nanoparticle tracking analysis and their association with
978 systemic lupus erythematosus. *Proc Natl Acad Sci U S A* 118:
979 Kaneko, N., H.H. Kuo, J. Boucau, J.R. Farmer, H. Allard-Chamard, V.S. Mahajan, A. Piechocka-
980 Trocha, K. Lefteri, M. Osborn, J. Bals, Y.C. Bartsch, N. Bonheur, T.M. Caradonna, J.
981 Chevalier, F. Chowdhury, T.J. Diefenbach, K. Einkauf, J. Fallon, J. Feldman, K.K. Finn, P.
982 Garcia-Broncano, C.A. Hartana, B.M. Hauser, C. Jiang, P. Kaplonek, M. Karpell, E.C.
983 Koscher, X. Lian, H. Liu, J. Liu, N.L. Ly, A.R. Michell, Y. Rassadkina, K. Seiger, L. Sessa, S.
984 Shin, N. Singh, W. Sun, X. Sun, H.J. Ticheli, M.T. Waring, A.L. Zhu, G. Alter, J.Z. Li, D.
985 Lingwood, A.G. Schmidt, M. Lichterfeld, B.D. Walker, X.G. Yu, R.F. Padera, Jr., S. Pillai,
986 and G. Massachusetts Consortium on Pathogen Readiness Specimen Working. 2020.
987 Loss of Bcl-6-Expressing T Follicular Helper Cells and Germinal Centers in COVID-19.
988 *Cell* 183:143-157 e113.
989 Karnell, J.L., M. Albulescu, S. Drabic, L. Wang, R. Moate, M. Baca, V. Oganesyan, M. Gunsior,
990 T. Thisted, L. Yan, J. Li, X. Xiong, S.C. Eck, M. de Los Reyes, I. Yusuf, K. Streicher, U.
991 Muller-Ladner, D. Howe, R. Ettinger, R. Herbst, and J. Drappa. 2019. A CD40L-targeting
992 protein reduces autoantibodies and improves disease activity in patients with
993 autoimmunity. *Sci Transl Med* 11:
994 Knight, J.S., R. Caricchio, J.L. Casanova, A.J. Combes, B. Diamond, S.E. Fox, D.A. Hanauer, J.A.
995 James, Y. Kanthi, V. Ladd, P. Mehta, A.M. Ring, I. Sanz, C. Selmi, R.P. Tracy, P.J. Utz,
996 C.A. Wagner, J.Y. Wang, and W.J. McCune. 2021. The intersection of COVID-19 and
997 autoimmunity. *J Clin Invest* 131:
998 Kumagai, T., T. Miki, M. Kikuchi, T. Fukuda, N. Miyasaka, R. Kamiyama, and S. Hirosawa. 1999.
999 The proto-oncogene Bc16 inhibits apoptotic cell death in differentiation-induced
1000 mouse myogenic cells. *Oncogene* 18:467-475.
1001 Kuraoka, M., A.G. Schmidt, T. Nojima, F. Feng, A. Watanabe, D. Kitamura, S.C. Harrison, T.B.
1002 Kepler, and G. Kelsoe. 2016. Complex Antigens Drive Permissive Clonal Selection in
1003 Germinal Centers. *Immunity* 44:542-552.
1004 Kurosu, T., T. Fukuda, T. Miki, and O. Miura. 2003. BCL6 overexpression prevents increase in
1005 reactive oxygen species and inhibits apoptosis induced by chemotherapeutic reagents
1006 in B-cell lymphoma cells. *Oncogene* 22:4459-4468.
1007 Kwon, K., C. Hutter, Q. Sun, I. Bilic, C. Cobaleda, S. Malin, and M. Busslinger. 2008. Instructive
1008 role of the transcription factor E2A in early B lymphopoiesis and germinal center B cell
1009 development. *Immunity* 28:751-762.
1010 Lau, C.M., C. Broughton, A.S. Tabor, S. Akira, R.A. Flavell, M.J. Mamula, S.R. Christensen, M.J.
1011 Shlomchik, G.A. Viglianti, I.R. Rifkin, and A. Marshak-Rothstein. 2005. RNA-associated
1012 autoantigens activate B cells by combined B cell antigen receptor/Toll-like receptor 7
1013 engagement. *J Exp Med* 202:1171-1177.

1014 Leadbetter, E.A., I.R. Rifkin, A.M. Hohlbaum, B.C. Beaudette, M.J. Shlomchik, and A. Marshak-
1015 Rothstein. 2002. Chromatin-IgG complexes activate B cells by dual engagement of IgM
1016 and Toll-like receptors. *Nature* 416:603-607.
1017 Lee, S.K., R.J. Rigby, D. Zotos, L.M. Tsai, S. Kawamoto, J.L. Marshall, R.R. Ramiscal, T.D. Chan,
1018 D. Gatto, R. Brink, D. Yu, S. Fagarasan, D.M. Tarlinton, A.F. Cunningham, and C.G.
1019 Vinuesa. 2011. B cell priming for extrafollicular antibody responses requires Bcl-6
1020 expression by T cells. *J Exp Med* 208:1377-1388.
1021 Luzina, I.G., S.P. Atamas, C.E. Storrer, L.C. daSilva, G. Kelsoe, J.C. Papadimitriou, and B.S.
1022 Handwerger. 2001. Spontaneous formation of germinal centers in autoimmune mice.
1023 *J Leukoc Biol* 70:578-584.
1024 Nojima, T., K. Haniuda, T. Moutai, M. Matsudaira, S. Mizokawa, I. Shiratori, T. Azuma, and D.
1025 Kitamura. 2011. In-vitro derived germinal centre B cells differentially generate
1026 memory B or plasma cells in vivo. *Nat Commun* 2:465.
1027 Paus, D., T.G. Phan, T.D. Chan, S. Gardam, A. Basten, and R. Brink. 2006. Antigen recognition
1028 strength regulates the choice between extrafollicular plasma cell and germinal center
1029 B cell differentiation. *J Exp Med* 203:1081-1091.
1030 Phan, R.T., and R. Dalla-Favera. 2004. The BCL6 proto-oncogene suppresses p53 expression in
1031 germinal-centre B cells. *Nature* 432:635-639.
1032 Psianou, K., I. Panagoulias, A.D. Papanastasiou, A.L. de Lastic, M. Rodi, P.I. Spantidea, S.E.
1033 Degn, P. Georgiou, and A. Mouzaki. 2018. Clinical and immunological parameters of
1034 Sjogren's syndrome. *Autoimmun Rev* 17:1053-1064.
1035 Rahman, A., and D.A. Isenberg. 2008. Systemic lupus erythematosus. *N Engl J Med* 358:929-
1036 939.
1037 Robinson, M.J., Z. Ding, C. Pitt, E.J. Brodie, I. Quast, D.M. Tarlinton, and D. Zotos. 2020. The
1038 Amount of BCL6 in B Cells Shortly after Antigen Engagement Determines Their
1039 Representation in Subsequent Germinal Centers. *Cell Rep* 30:1530-1541 e1534.
1040 Roco, J.A., L. Mesin, S.C. Binder, C. Nefzger, P. Gonzalez-Figueroa, P.F. Canete, J. Ellyard, Q.
1041 Shen, P.A. Robert, J. Cappello, H. Vohra, Y. Zhang, C.R. Nowosad, A. Schiepers, L.M.
1042 Corcoran, K.M. Toellner, J.M. Polo, M. Meyer-Hermann, G.D. Victora, and C.G.
1043 Vinuesa. 2019. Class-Switch Recombination Occurs Infrequently in Germinal Centers.
1044 *Immunity* 51:337-350 e337.
1045 Soni, C., O.A. Perez, W.N. Voss, J.N. Pucella, L. Serpas, J. Mehl, K.L. Ching, J. Goike, G. Georgiou,
1046 G.C. Ippolito, V. Sisirak, and B. Reizis. 2020. Plasmacytoid Dendritic Cells and Type I
1047 Interferon Promote Extrafollicular B Cell Responses to Extracellular Self-DNA.
1048 *Immunity* 52:1022-1038 e1027.
1049 Sweet, R.A., S.R. Christensen, M.L. Harris, J. Shupe, J.L. Sutherland, and M.J. Shlomchik. 2010.
1050 A new site-directed transgenic rheumatoid factor mouse model demonstrates
1051 extrafollicular class switch and plasmablast formation. *Autoimmunity* 43:607-618.
1052 Sweet, R.A., M.L. Ols, J.L. Cullen, A.V. Milam, H. Yagita, and M.J. Shlomchik. 2011. Facultative
1053 role for T cells in extrafollicular Toll-like receptor-dependent autoreactive B-cell
1054 responses in vivo. *Proc Natl Acad Sci U S A* 108:7932-7937.
1055 Toellner, K.M., A. Gulbranson-Judge, D.R. Taylor, D.M. Sze, and I.C. MacLennan. 1996.
1056 Immunoglobulin switch transcript production in vivo related to the site and time of
1057 antigen-specific B cell activation. *J Exp Med* 183:2303-2312.
1058 Vasanwala, F.H., S. Kusam, L.M. Toney, and A.L. Dent. 2002. Repression of AP-1 function: a
1059 mechanism for the regulation of Blimp-1 expression and B lymphocyte differentiation
1060 by the B cell lymphoma-6 protooncogene. *J Immunol* 169:1922-1929.

1061 Victora, G.D., and M.C. Nussenzweig. 2022. Germinal Centers. *Annu Rev Immunol*
1062 Weening, J.J., V.D. D'Agati, M.M. Schwartz, S.V. Seshan, C.E. Alpers, G.B. Appel, J.E. Balow,
1063 J.A. Bruijn, T. Cook, F. Ferrario, A.B. Fogo, E.M. Ginzler, L. Hebert, G. Hill, P. Hill, J.C.
1064 Jennette, N.C. Kong, P. Lesavre, M. Lockshin, L.M. Looi, H. Makino, L.A. Moura, and M.
1065 Nagata. 2004. The classification of glomerulonephritis in systemic lupus
1066 erythematosus revisited. *J Am Soc Nephrol* 15:241-250.
1067 William, J., C. Euler, S. Christensen, and M.J. Shlomchik. 2002. Evolution of autoantibody
1068 responses via somatic hypermutation outside of germinal centers. *Science* 297:2066-
1069 2070.
1070 Wittenborn, T.R., C. Fahlquist Hagert, A. Ferapontov, S. Fonager, L. Jensen, G. Winther, and
1071 S.E. Degn. 2021. Comparison of gamma and x-ray irradiation for myeloablation and
1072 establishment of normal and autoimmune syngeneic bone marrow chimeras. *PLoS*
1073 *One* 16:e0247501.
1074 Woodruff, M.C., R.P. Ramonell, D.C. Nguyen, K.S. Cashman, A.S. Saini, N.S. Haddad, A.M. Ley,
1075 S. Kyu, J.C. Howell, T. Ozturk, S. Lee, N. Suryadevara, J.B. Case, R. Bugrovsky, W. Chen,
1076 J. Estrada, A. Morrison-Porter, A. Derrico, F.A. Anam, M. Sharma, H.M. Wu, S.N. Le,
1077 S.A. Jenks, C.M. Tipton, B. Staitieh, J.L. Daiss, E. Ghosn, M.S. Diamond, R.H. Carnahan,
1078 J.E. Crowe, Jr., W.T. Hu, F.E. Lee, and I. Sanz. 2020. Extrafollicular B cell responses
1079 correlate with neutralizing antibodies and morbidity in COVID-19. *Nat Immunol*
1080 21:1506-1516.
1081 Yokogawa, M., M. Takaishi, K. Nakajima, R. Kamijima, C. Fujimoto, S. Kataoka, Y. Terada, and
1082 S. Sano. 2014. Epicutaneous application of toll-like receptor 7 agonists leads to
1083 systemic autoimmunity in wild-type mice: a new model of systemic Lupus
1084 erythematosus. *Arthritis Rheumatol* 66:694-706.
1085 Zhang, Y., M. Meyer-Hermann, L.A. George, M.T. Figge, M. Khan, M. Goodall, S.P. Young, A.
1086 Reynolds, F. Falciani, A. Waisman, C.A. Notley, M.R. Ehrenstein, M. Kosco-Vilbois, and
1087 K.M. Toellner. 2013. Germinal center B cells govern their own fate via antibody
1088 feedback. *J Exp Med* 210:457-464.
1089